

LA-UR-19-29577

Approved for public release; distribution is unlimited.

Title: The virtual element method for linear elastodynamics models. Design, analysis, and implementation

Author(s): Manzini, Gianmarco
Mourad, Hashem Mohamed
Antonietti, Paola Francesca
Verani, Marco

Intended for: Report

Issued: 2020-09-27 (rev.1)

Disclaimer:

Los Alamos National Laboratory, an affirmative action/equal opportunity employer, is operated by Triad National Security, LLC for the National Nuclear Security Administration of U.S. Department of Energy under contract 89233218CNA000001. By approving this article, the publisher recognizes that the U.S. Government retains nonexclusive, royalty-free license to publish or reproduce the published form of this contribution, or to allow others to do so, for U.S. Government purposes. Los Alamos National Laboratory requests that the publisher identify this article as work performed under the auspices of the U.S. Department of Energy. Los Alamos National Laboratory strongly supports academic freedom and a researcher's right to publish; as an institution, however, the Laboratory does not endorse the viewpoint of a publication or guarantee its technical correctness.

The virtual element method for linear elastodynamics models. Design, analysis, and implementation

P. F. Antonietti ^a, G. Manzini ^b, H. M. Mourad ^c, and M. Verani ^d

^a *MOX, Dipartimento di Matematica, Politecnico di Milano, Italy; e-mail: paola.antonietti@polimi.it*

^b *Group T-5, Theoretical Division, Los Alamos National Laboratory, Los Alamos, NM, USA; e-mail: gmanzini@lanl.gov*

^c *Group T-3, Theoretical Division, Los Alamos National Laboratory, Los Alamos, NM, USA; e-mail: hmourad@lanl.gov*

^d *MOX, Dipartimento di Matematica, Politecnico di Milano, Italy; e-mail: marco.verani@polimi.it*

Abstract

We design the conforming virtual element method for the numerical simulation of two dimensional time-dependent elastodynamics problems. We investigate the performance of the method both theoretically and numerically. We prove the stability and the convergence of the semi-discrete approximation in the energy norm and derive optimal error estimates. We also show the convergence in the L^2 norm. The performance of the virtual element method is assessed on a set of different computational meshes, including non-convex cells up to order four in the h -refinement setting. Exponential convergence is also experimentally seen in the p -refinement setting.

Key words: virtual element method, polytopal mesh, elastodynamics, high-order methods

1. Introduction

In recent years, numerical modeling of elastic waves propagation problems through the elastodynamics equation has undergone a constantly increasing interest in the mathematical and geophysics engineering community. One of the first numerical methods was based on finite differences, see, e.g., [8, 75, 97] and [92] for a comprehensive review. Spectral and pseudo-spectral formulations have also been employed for the elastodynamics equation [81, 84, 85, 118]. To improve the geometric flexibility while preserving accuracy, spectral element methods have successfully been applied to the elastodynamics equation, cf. [72, 73, 83, 103, 107]. See, also, [77, 109, 113] for spectral methods on tensor-product grids and the extension to tetrahedral and/or hybrid meshes based on employing nodal (or Lagrangian) basis functions associated to suitable interpolation points. Elastic waves propagation problems have been treated numerically by applying the Discontinuous Galerkin (DG) and the Discontinuous Galerkin Spectral Element method [9, 10, 15, 65, 74, 106] to the *displacement formulation* and the *stress-velocity formulation* [71, 82]. High-order DG methods for elastic and elasto-acoustic wave propagation problems have been extended to arbitrarily-shaped polygonal/polyhedral grids [12, 14] to further enhance the geometrical flexibility of the DG approach while guaranteeing low dissipation and dispersion errors.

Studying the elastodynamic behavior of structures with complicated geometrical features is often of interest in many practical situations, e.g., in aerospace and power-generation applications. Traditionally, triangular—and in 3D, tetrahedral—elements have been the only available option when it came to the spatial discretization of such structures. This is problematic because low-order triangles/tetrahedra are known to over-estimate the structure's stiffness (and hence its natural frequencies and the wave propagation speed within it), especially with nearly-incompressible

materials such as rubber, or in the presence of well-developed (isochoric) plastic flow in metals [58, 68, 112]. In addition, very small triangular elements are often needed to resolve intricate features of the geometry, which then requires a very small time step to be used in view of the CFL stability condition [63]. Polygonal elements can alleviate such difficulties, since they often obviate the need to refine the spatial discretization even in the presence of complicated/intricate geometrical features. This is especially true if the underlying numerical method allows *non-convex* polygonal elements to be used efficiently, as is the case with the virtual element method (VEM); e.g., see [61].

We are aimed, here, at investigating the use of the virtual element method for numerical modeling wave propagation phenomena in elastic media. To this end, we consider the conforming virtual element method (VEM) that was proved to be successful for simple parabolic and hyperbolic problems [1, 2, 110, 111]. We also mention a first work in this direction, see Ref. [98, 99], where the low-order virtual element method is applied to nonconvex polygonal meshes.

The VEM was originally proposed for solving elliptic boundary-value problems on polytopal meshes in [18, 20]. The central idea is that the basis functions are defined as the solution of a local elliptic partial differential equation and are never explicitly computed in the practical implementation of the method. For this reason, they are dubbed as *virtual*, and the finite element space of the VEM is called the *virtual element space*. Instead of computing the basis functions, the VEM uses their elliptic polynomial projections to compute approximate bilinear forms (stiffness and mass matrices) and the continuous linear functional expressing the loading term. Such projections are computable from the degrees of freedom without introducing any further approximation error and are used to decompose the bilinear form at the elemental level into two parts: the consistent term that approximates the stiffness matrix on a given polynomial space and the correction term that ensures stability. As in finite elements, element-level assembly procedures are used to obtain the discrete system of linear equations.

The outline of the paper is as follows. We conclude this introductory section with a subsection reviewing background material for the VEM and a subsection introducing the notation used in this paper. In Section 2 we introduce the model problem and its virtual element approximation. In Section 3 we present the design of the VEM. In Section 4 we discuss the convergence of the VEM and we derive the error estimates. In Section 5 we investigate the performance of the method on a set of suitable numerical experiments. In Section 6 we offer our final remarks and conclusions.

1.1. Background material on the VEM

The VEM was originally developed as a variational reformulation of the *nodal* mimetic finite difference (MFD) method [29, 36, 48, 88] for solving diffusion problems on unstructured polygonal meshes. A survey on the MFD method can be found in the review paper [87] and the research monograph [30]. The VEM inherits the flexibility of the MFD method with respect to the admissible meshes and this feature is well reflected in the many significant applications that have been developed so far, see, for example, [11, 21–28, 31, 33–35, 38–46, 49, 51, 94, 95, 100, 101, 111, 117]. Moreover, the connection between VEM and finite elements on polygonal/polyhedral meshes is thoroughly investigated in [54, 70, 89], and between VEM and BEM-based FEM method in [53]. The VEM was originally formulated in [20] as a conforming FEM for the Poisson problem. It was later extended to convection-reaction-diffusion problems with variable coefficients in [5, 27]. Meanwhile, the nonconforming formulation for diffusion problems was proposed in [18] as the finite element reformulation of [86] and later extended to general elliptic problems [56], Stokes problem [52], and the biharmonic equation [13, 121].

In the most recent years, a great amount of work has also been devoted to the development of approximation methods for the numerical modeling of linear and nonlinear elasticity problems and materials. VEM for plate bending problems [21, 49] and stress/displacement VEM for plane elasticity problems [16], plane elasticity problems based on the Hellinger-Reissner principle [17], two-dimensional mixed weakly symmetric formulation of linear elasticity [119], mixed virtual element method for a pseudostress-based formulation of linear elasticity [50] nonconforming virtual element method for elasticity problems [120], linear [76] and nonlinear elasticity [66], contact problems [117] and frictional contact problems including large deformations [116], elastic and inelastic problems on polytope meshes [31], compressible and incompressible finite deformations [115], finite elasto-plastic deformations [59, 78, 114], linear elastic fracture analysis [96], phase-field modeling of brittle fracture using an efficient virtual element scheme [6] and ductile fracture [7], crack propagation [80], brittle crack-propagation [79], large strain anisotropic material with inextensive fibers [108], isotropic damage [67], computational homogenization of polycrystalline materials [90], gradient recovery scheme [60], topology optimization [62], nonconvex meshes for elastodynamics [98, 99], acoustic vibration

problem [37], virtual element method for coupled thermo-elasticity in Abaqus [69], a priori and a posteriori error estimates for a virtual element spectral analysis for the elasticity equations [93], virtual element method for transversely isotropic elasticity [105].

1.2. Notation of functional spaces and technicalities

We use the standard definition and notation of Sobolev spaces, norms and seminorms, cf. [4]. Let k be a nonnegative integer number. The Sobolev space $H^k(\omega)$ consists of all square integrable functions with all square integrable weak derivatives up to order k that are defined on the open bounded connected subset ω of \mathbb{R}^2 . As usual, if $k = 0$, we prefer the notation $L^2(\omega)$. Norm and seminorm in $H^k(\omega)$ are denoted by $\|\cdot\|_{k,\omega}$ and $|\cdot|_{k,\omega}$, respectively, and $(\cdot, \cdot)_\omega$ denote the L^2 -inner product. We omit the subscript ω when ω is the whole computational domain Ω .

Given the mesh partitioning $\Omega_h = \{\mathbf{P}\}$ of the domain Ω into elements \mathbf{P} , we define the broken (scalar) Sobolev space for any integer $k > 0$

$$H^k(\Omega_h) = \prod_{\mathbf{P} \in \Omega_h} H^k(\mathbf{P}) = \{ v \in L^2(\Omega) : v|_{\mathbf{P}} \in H^k(\mathbf{P}) \},$$

which we endow with the broken H^k -norm

$$\|v\|_{k,h}^2 = \sum_{\mathbf{P} \in \Omega_h} \|v\|_{k,\mathbf{P}}^2 \quad \forall v \in H^k(\Omega_h), \quad (1)$$

and, for $k = 1$, with the broken H^1 -seminorm

$$|v|_{1,h}^2 = \sum_{\mathbf{P} \in \Omega_h} \|\nabla v\|_{0,\mathbf{P}}^2 \quad \forall v \in H^1(\Omega_h). \quad (2)$$

We denote the linear space of polynomials of degree up to ℓ defined on ω by $\mathbb{P}_\ell(\omega)$, with the useful conventional notation that $\mathbb{P}_{-1}(\omega) = \{0\}$. We denote the space of two-dimensional vector polynomials of degree up to ℓ on ω by $[\mathbb{P}_\ell(\omega)]^2$; the space of symmetric 2×2 -sized tensor polynomials of degree up to ℓ on ω by $\mathbb{P}_{\ell,\text{sym}}^{2 \times 2}(\omega)$. Space $\mathbb{P}_\ell(\omega)$ is the span of the finite set of *scaled monomials of degree up to ℓ* , that are given by

$$\mathcal{M}_\ell(\omega) = \left\{ \left(\frac{\mathbf{x} - \mathbf{x}_\omega}{h_\omega} \right)^\alpha \text{ with } |\alpha| \leq \ell \right\},$$

where

- \mathbf{x}_ω denotes the center of gravity of ω and h_ω its characteristic length, as, for instance, the edge length or the cell diameter for $d = 1, 2, 3$;
- $\alpha = (\alpha_1, \alpha_2)$ is the two-dimensional multi-index of nonnegative integers α_i with degree $|\alpha| = \alpha_1 + \alpha_2 \leq \ell$ and such that $\mathbf{x}^\alpha = x_1^{\alpha_1} x_2^{\alpha_2}$ for any $\mathbf{x} \in \mathbb{R}^2$.

We will also use the set of *scaled monomials of degree exactly equal to ℓ* , denoted by $\mathcal{M}_\ell^*(\omega)$ and obtained by setting $|\alpha| = \ell$ in the definition above.

Finally, we use the letter C in the error estimates to denote a strictly positive constant whose value can change at any instance and that is independent of the discretization parameters such as the mesh size h . Note that C may depend on the constants of the model equations or the variational problem, like the coercivity and continuity constants, or even constants that are uniformly defined for the family of meshes of the approximation while $h \rightarrow 0$, such as the mesh regularity constant, the stability constants of the discrete bilinear forms, etc. Whenever it is convenient, we will simplify the notation by using expressions like $x \lesssim y$ and $x \gtrsim y$ to mean that $x \leq Cy$ and $x \geq Cy$, respectively, C being the generic constant in the sense defined above.

2. Model problem and virtual element formulation

We consider an elastic body occupying the open, bounded polygonal domain denoted by $\Omega \in \mathbb{R}^2$ with boundary denoted by $\Gamma = \partial\Omega$. We assume that boundary Γ can be split into the two disjoint subsets Γ_D and Γ_N , so that $\overline{\Gamma} = \overline{\Gamma}_D \cup \overline{\Gamma}_N$ and $\Gamma_D \cap \Gamma_N = \emptyset$. For the well-posedness of the mathematical model, we further require that the

one-dimensional Lebesgue measure (length) of Γ_D is nonzero, i.e., $|\Gamma_D| > 0$. Let $T > 0$ denote the final time. We consider the external load $\mathbf{f} \in L^2((0, T); [L^2(\Omega)]^2)$, the boundary function $\mathbf{g}_N \in C^1((0, T); [H_{0, \Gamma_N}^{\frac{1}{2}}]^2)$, and the initial functions $\mathbf{u}_0 \in [H_{0, \Gamma_D}^1(\Omega)]^2$, $\mathbf{u}_1 \in [L^2(\Omega)]^2$. For such time-dependent vector fields, we may indicate the dependence on time explicitly, e.g., $\mathbf{f}(t) := \mathbf{f}(\cdot, t) \in [L^2(\Omega)]^2$, or drop it out to ease the notation when it is obvious from the context.

The equations governing the two-dimensional initial/boundary-value problem of linear elastodynamics for the displacement vector $\mathbf{u} : \Omega \times [0, T] \rightarrow \mathbb{R}^2$ are:

$$\rho \ddot{\mathbf{u}} - \nabla \cdot \boldsymbol{\sigma}(\mathbf{u}) = \mathbf{f} \quad \text{in } \Omega \times (0, T], \quad (3)$$

$$\mathbf{u} = \mathbf{0} \quad \text{on } \Gamma_D \times (0, T], \quad (4)$$

$$\boldsymbol{\sigma}(\mathbf{u})\mathbf{n} = \mathbf{g}_N \quad \text{on } \Gamma_N \times (0, T], \quad (5)$$

$$\mathbf{u} = \mathbf{u}_0 \quad \text{in } \Omega \times \{0\}, \quad (6)$$

$$\dot{\mathbf{u}} = \mathbf{u}_1 \quad \text{in } \Omega \times \{0\}. \quad (7)$$

Here, ρ is the mass density, which we suppose to be a strictly positive and uniformly bounded function and $\boldsymbol{\sigma}(\mathbf{u})$ is the stress tensor. In (4) we assume homogeneous Dirichlet boundary conditions on Γ_D . This assumption is made only to ease the exposition and the analysis, as our numerical method is easily extendable to treat the case of nonhomogeneous Dirichlet boundary conditions.

We denote the space of symmetric 2×2 -sized real-valued tensors by $\mathbb{R}_{\text{sym}}^{2 \times 2}$ and assume that the stress tensor $\boldsymbol{\sigma} : \Omega \times [0, T] \rightarrow \mathbb{R}_{\text{sym}}^{2 \times 2}$ is expressed, according to Hooke's law, by $\boldsymbol{\sigma}(\mathbf{u}) = \mathcal{D}\boldsymbol{\varepsilon}(\mathbf{u})$, where, $\boldsymbol{\varepsilon}(\mathbf{u})$ denotes the symmetric gradient of \mathbf{u} , i.e., $\boldsymbol{\varepsilon}(\mathbf{u}) = (\nabla \mathbf{u} + (\nabla \mathbf{u})^T)/2$, and $\mathcal{D} = \mathcal{D}(\mathbf{x}) : \mathbb{R}_{\text{sym}}^{2 \times 2} \rightarrow \mathbb{R}_{\text{sym}}^{2 \times 2}$ is the inverse of the *compliance* tensor

$$\mathcal{D}\boldsymbol{\tau} = 2\mu\boldsymbol{\tau} + \lambda \text{tr}(\boldsymbol{\tau})\mathbf{I} \quad (8)$$

for all $\boldsymbol{\tau} \in \mathbb{R}_{\text{sym}}^{2 \times 2}$. In this definition, \mathbf{I} and $\text{tr}(\cdot)$ are the identity matrix and the trace operator; λ and μ are the first and second Lamé coefficients, that we assume to be in $L^\infty(\Omega)$ and nonnegative.

Let $\mathbf{V} = [H_{\Gamma_D}^1(\Omega)]^2$ be the space of H^1 vector valued functions with null trace on Γ_D . We consider the two bilinear forms $m(\cdot, \cdot)$, $a(\cdot, \cdot) : \mathbf{V} \times \mathbf{V} \rightarrow \mathbb{R}$ defined as

$$m(\mathbf{w}, \mathbf{v}) = \int_{\Omega} \rho \mathbf{w} \cdot \mathbf{v} \, dV \quad \forall \mathbf{w}, \mathbf{v} \in \mathbf{V}, \quad (9)$$

$$a(\mathbf{w}, \mathbf{v}) = \int_{\Omega} \boldsymbol{\sigma}(\mathbf{w}) : \boldsymbol{\varepsilon}(\mathbf{v}) \, dV \quad \forall \mathbf{w}, \mathbf{v} \in \mathbf{V}, \quad (10)$$

and the linear functional $F(\cdot) : \mathbf{V} \rightarrow \mathbb{R}$ defined as

$$F(\mathbf{v}) = \int_{\Omega} \mathbf{f} \cdot \mathbf{v} \, dV + \int_{\Gamma_N} \mathbf{g}_N \cdot \mathbf{v} \quad \forall \mathbf{v} \in \mathbf{V}. \quad (11)$$

The variational formulation of the linear elastodynamics equations reads as: *For all $t \in (0, T]$ find $\mathbf{u}(t) \in \mathbf{V}$ such that for $t = 0$ it holds that $\mathbf{u}(0) = \mathbf{u}_0$ and $\dot{\mathbf{u}}(0) = \mathbf{u}_1$ and*

$$m(\ddot{\mathbf{u}}, \mathbf{v}) + a(\mathbf{u}, \mathbf{v}) = F(\mathbf{v}) \quad \forall \mathbf{v} \in \mathbf{V}. \quad (12)$$

As shown, for example, in [104, Theorem 8-3.1], the variational problem (12) is well posed and its unique solution satisfies $\mathbf{u} \in C^0((0, T]; \mathbf{V}) \cap C^1((0, T]; [L^2(\Omega)]^2)$.

The virtual element approximation of problem (12) relies on the virtual element space \mathbf{V}_k^h , which is a subspace of $[H_{\Gamma_D}^1(\Omega)]^2$. Space \mathbf{V}_k^h is built upon the scalar conforming space considered in [20]. For the sake of completeness, we briefly review the construction of the scalar space in the next section. Then, we consider the virtual element bilinear forms $m_h(\cdot, \cdot)$ and $a_h(\cdot, \cdot)$, which approximate the bilinear forms $m(\cdot, \cdot)$ and $a(\cdot, \cdot)$, and the virtual element functional

$F_h(\cdot)$, which approximates the linear functional $F(\cdot)$. The definition of $m_h(\cdot, \cdot)$, $a_h(\cdot, \cdot)$, and $F_h(\cdot)$ and the discussion of their properties is addressed in the next section.

The semi-discrete virtual element approximation of (12) read as: *For all $t \in (0, T]$ find $\mathbf{u}_h(t) \in \mathbf{V}_k^h$ such that for $t = 0$ it holds that $\mathbf{u}_h(0) = (\mathbf{u}_0)_I$ and $\dot{\mathbf{u}}_h(0) = (\mathbf{u}_1)_I$ and*

$$m_h(\ddot{\mathbf{u}}_h, \mathbf{v}_h) + a_h(\mathbf{u}_h, \mathbf{v}_h) = F_h(\mathbf{v}_h) \quad \forall \mathbf{v}_h \in \mathbf{V}_k^h. \quad (13)$$

Here, $\mathbf{u}_h(t)$ is the virtual element approximation of \mathbf{u} and \mathbf{v}_h the generic test function in \mathbf{V}_k^h , while $(\mathbf{u}_0)_I$ and $(\mathbf{u}_1)_I$ are the virtual element interpolants of the initial solution functions $\mathbf{u}(0)$ and $\dot{\mathbf{u}}(0)$, respectively.

Time integration is performed by applying the leap-frog time marching scheme [102] to the second derivative in time $\ddot{\mathbf{u}}_h$. To this end, we subdivide the interval $(0, T]$ into N_T subintervals of amplitude $\Delta t = T/N_T$ and at every time level $t^n = n\Delta t$ we consider the variational problem:

$$m_h(\mathbf{u}_h^{n+1}, \mathbf{v}_h) - 2m_h(\mathbf{u}_h^n, \mathbf{v}_h) + m_h(\mathbf{u}_h^{n-1}, \mathbf{v}_h) + \Delta t a_h(\mathbf{u}_h^n, \mathbf{v}_h) = \Delta t F_h^n(\mathbf{v}_h) \quad \forall \mathbf{v}_h \in \mathbf{V}_k^h. \quad (14)$$

The leap-frog scheme is second-order accurate, explicit and conditionally stable, cf. [102]. It is straightforward to show that these properties are inherited by the fully-discrete scheme (14).

3. Virtual Element Approximation

The VEM proposed in this paper is a vector extension of the VEM previously developed for scalar elliptic and parabolic problems in [5, 18, 20, 56], that we shortly review in this section. First, we introduce the family of mesh decompositions of the computational domain and the mesh regularity assumptions needed to prove the stability and convergence of the method. Then, we formulate the conforming virtual element spaces of various degree k and present the degrees of the freedom that are unisolvant in such spaces. Finally, we present the definition of the virtual element bilinear forms and discuss their properties.

3.1. Mesh definition and regularity assumptions

Let $\mathcal{T} = \{\Omega_h\}_h$ be a family of decompositions of Ω into nonoverlapping polygonal elements \mathbf{P} with nonintersecting boundary $\partial\mathbf{P}$, center of gravity $\mathbf{x}_\mathbf{P}$, two-dimensional measure (area) $|\mathbf{P}|$, and diameter $h_\mathbf{P} = \sup_{\mathbf{x}, \mathbf{y} \in \mathbf{P}} |\mathbf{x} - \mathbf{y}|$. The subindex h that labels each mesh Ω_h is the maximum of the diameters $h_\mathbf{P}$ of the elements of that mesh. The boundary of \mathbf{P} is formed by straight edges e and the midpoint and length of each edge are denoted by \mathbf{x}_e and h_e , respectively.

We denote the unit normal vector to the elemental boundary $\partial\mathbf{P}$ by $\mathbf{n}_\mathbf{P}$, and the unit normal vector to edge e by \mathbf{n}_e . Vector $\mathbf{n}_\mathbf{P}$ points out of \mathbf{P} and the orientation of \mathbf{n}_e is fixed *once and for all* in every mesh.

Now, we state the mesh regularity assumptions that are required for the convergence analysis.

(A0) Mesh regularity assumptions.

- There exists a positive constant ϱ independent of h (and, hence, of Ω_h) such that for every polygonal element $\mathbf{P} \in \Omega_h$ it holds that
 - (i) \mathbf{P} is star-shaped with respect to a disk with radius $\geq \varrho h_\mathbf{P}$;
 - (ii) for every edge $e \in \partial\mathbf{P}$ it holds that $h_e \geq \varrho h_\mathbf{P}$.

Remark 3.1 *Star-shapedness property (i) implies that the elements are simply connected subsets of \mathbb{R}^2 . Scaling property (ii) implies that the number of edges in each elemental boundary is uniformly bounded over the whole mesh family \mathcal{T} .*

To conclude this section, we note that the above mesh assumptions are very general and, as observed from the first publications on the VEM, see, for example, [20], allow us to formulate the VEM on grids of polygonal elements having very general geometric shapes, e.g., nonconvex elements or elements with hanging nodes. See also the recent work [32] for weaker mesh assumptions.

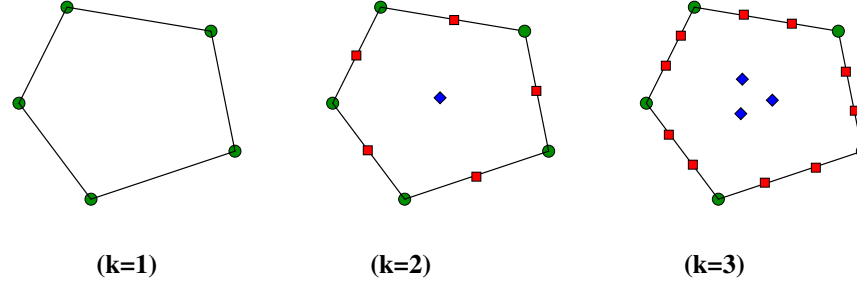


Fig. 1. The degrees of freedom of the scalar conforming virtual element spaces $V_k^h(\mathbf{P})$ defined on the pentagonal cell \mathbf{P} for $k = 1, 2, 3$.

3.2. Virtual element space, degrees of freedom and projection operators

The global virtual element space is defined as

$$\mathbf{V}_k^h := \left\{ \mathbf{v} \in \mathbf{V} : \mathbf{v}|_{\mathbf{P}} \in \mathbf{V}_k^h(\mathbf{P}) \text{ for every } \mathbf{P} \in \Omega_h \right\}. \quad (15)$$

The construction of the local virtual space is carried out along these three steps: (i) we select the set of degrees of freedom that uniquely characterizes the functions of the local space; (ii) we introduce the elliptic projector onto the subspace of polynomials; (iii) we define the virtual element functions as the solution of a differential problem, also using the elliptic projector.

Let us move to the first step.

- Each virtual element function v_h is uniquely characterized by
 - (C1) the values of v_h at the vertices of \mathbf{P} ;
 - (C2) the moments of v_h of order up to $k - 1$ on each one-dimensional edge $e \in \partial\mathbf{P}$:

$$\frac{1}{|e|} \int_e v_h m \, ds, \quad \forall m \in \mathcal{M}_{k-1}(e), \quad \forall e \in \partial\mathbf{P}; \quad (16)$$

- (C3) the moments of v_h of order up to $k - 2$ on \mathbf{P} :

$$\frac{1}{|\mathbf{P}|} \int_{\mathbf{P}} v_h m \, ds, \quad \forall m \in \mathcal{M}_{k-2}(\mathbf{P}). \quad (17)$$

Figure 1 shows the degrees of freedom of the three scalar conforming virtual element spaces defined on a pentagonal cell for $k = 1, 2, 3$. Since we assume that $\mathbf{V}_k^h(\mathbf{P}) = [V_k^h(\mathbf{P})]^2$, being $V_k^h(\mathbf{P})$ the local scalar conforming virtual space, the degrees of freedom of each component of the vector-valued functions \mathbf{v}_h are those described above.

In the second step, we introduce the elliptic projection operator $\Pi_k^{\nabla} : H^1(\mathbf{P}) \cap C^0(\bar{\mathbf{P}}) \rightarrow \mathbb{P}_k(\mathbf{P})$, so that the elliptic projection of a function v_h is the polynomial of degree k that satisfies the variational problem given by

$$\int_{\mathbf{P}} \nabla \Pi_k^{\nabla} v_h \cdot \nabla q_k \, dV = \int_{\mathbf{P}} \nabla v_h \cdot \nabla q_k \, dV \quad \forall q \in \mathbb{P}_k(\mathbf{P}), \quad (18)$$

with the additional condition that

$$\int_{\partial\mathbf{P}} \Pi_1^{\nabla} v_h \, dV = \int_{\partial\mathbf{P}} v_h \, dV \quad \text{for } k = 1, \quad (19)$$

$$\int_{\mathbf{P}} \Pi_k^{\nabla} v_h \, dV = \int_{\mathbf{P}} v_h \, dV \quad \text{for } k \geq 2. \quad (20)$$

The crucial property is that $\Pi_k^{\nabla} v_h$ is computable using only the information on v_h provided by its degrees of freedom, i.e., the values of the linear functionals (C1)-(C3).

In the third and final step, we define the conforming virtual element space of order $k \geq 1$ by

$$V_k^h(\mathbf{P}) := \left\{ v_h \in H^1(\mathbf{P}) : v_h|_{\partial\mathbf{P}} \in C(\partial\mathbf{P}), v_h|_e \in \mathbb{P}_k(e) \forall e \in \partial\mathbf{P}, \right. \\ \left. \Delta v_h \in \mathbb{P}_k(\mathbf{P}), (v_h - \Pi_k^\nabla v_h, \mu_h)_\mathbf{P} = 0 \quad \forall \mu_h \in \mathbb{P}_k(\mathbf{P}) \setminus \mathbb{P}_{k-2}(\mathbf{P}) \right\}. \quad (21)$$

Remark 3.2 *A few remarkable facts characterize these scalar functional spaces:*

- (i) *their definition resorts to the enhancement strategy introduced in [5] for the conforming VEM;*
- (ii) *the degrees of freedom (C1)-(C3) are unisolvant in $V_k^h(\mathbf{P})$, cf. [20];*
- (iii) *the scalar polynomial space $\mathbb{P}_k(\mathbf{P})$ is a subset of both $V_k^h(\mathbf{P})$;*
- (iv) *the L^2 -orthogonal projections $\Pi_k^0 v_h \in \mathbb{P}_k(\mathbf{P})$ and $\Pi_{k-1}^0 \nabla v_h \in [\mathbb{P}_{k-1}(\mathbf{P})]^2$ are computable for all $v_h \in V_k^h$ using only the degrees of freedom of v_h .*

From (iv), we readily find that for all $\mathbf{v}_h \in \mathbf{V}_k^h$ the L^2 -orthogonal projections $\Pi_k^0 \mathbf{v}_h \in [\mathbb{P}_k(\mathbf{P})]^2$ and $\Pi_{k-1}^0 \boldsymbol{\varepsilon}(\mathbf{v}_h) \in \mathbb{P}_{k-1,\text{sym}}^{2 \times 2}(\mathbf{P})$ are also computable (without any approximation) using only the degrees of freedom of \mathbf{v}_h . In particular, the latter one is the solution of the finite dimensional variational problem:

$$\int_{\mathbf{P}} \Pi_{k-1}^0(\boldsymbol{\varepsilon}(\mathbf{v}_h)) : \boldsymbol{\varepsilon}^p \, dV = \int_{\mathbf{P}} \boldsymbol{\varepsilon}(\mathbf{v}_h) : \boldsymbol{\varepsilon}^p \, dV \quad \forall \boldsymbol{\varepsilon}^p \in \mathbb{P}_{k-1,\text{sym}}^{2 \times 2}(\mathbf{P}), \quad (22)$$

i.e., the L^2 -projection of the symmetric gradient $\boldsymbol{\varepsilon}(\mathbf{v}_h)$ onto $\mathbb{P}_{k-1,\text{sym}}^{2 \times 2}(\mathbf{P})$, that (we recall) is the space of symmetric 2×2 -sized tensor-valued polynomials of degree up to $k-1$.

Finally, the degrees of freedom of the global space \mathbf{V}_k^h are provided by collecting all the local degrees of freedom. We note that the value of vertex degrees of freedom is the same for all the elements to which the vertex belongs. Similarly, the value of the edge degrees of freedom at internal edges (i.e., shared by two mesh elements) is the same for the two elements to which this edge belongs. The unisolvence of such degrees of freedom for the global space \mathbf{V}_k^h is an immediate consequence of the unisolvence of the local degrees of freedom for the elemental spaces $V_k^h(\mathbf{P})$.

3.3. Virtual element bilinear forms

In the virtual element setting, we define the bilinear forms $m_h(\cdot, \cdot)$ and $a_h(\cdot, \cdot)$ as the sum of elemental contributions, which are denoted by $m_h^P(\cdot, \cdot)$ and $a_h^P(\cdot, \cdot)$, respectively:

$$m_h(\cdot, \cdot) : \mathbf{V}_k^h \times \mathbf{V}_k^h \rightarrow \mathbb{R}, \quad \text{with} \quad m_h(\mathbf{w}_h, \mathbf{v}_h) = \sum_{\mathbf{P} \in \Omega_h} m_h^P(\mathbf{w}_h, \mathbf{v}_h), \\ a_h(\cdot, \cdot) : \mathbf{V}_k^h \times \mathbf{V}_k^h \rightarrow \mathbb{R}, \quad \text{with} \quad a_h(\mathbf{w}_h, \mathbf{v}_h) = \sum_{\mathbf{P} \in \Omega_h} a_h^P(\mathbf{w}_h, \mathbf{v}_h). \quad (23)$$

The local bilinear form $m_h^P(\cdot, \cdot)$ is given by

$$m_h^P(\mathbf{v}_h, \mathbf{w}_h) = \int_{\mathbf{P}} \rho \Pi_k^0 \mathbf{v}_h \cdot \Pi_k^0 \mathbf{w}_h \, dV + S_m^P(\mathbf{v}_h, \mathbf{w}_h), \quad (24)$$

where $S_m^P(\cdot, \cdot)$ is the local stabilization term. The bilinear form m_h^P depends on the orthogonal projections $\Pi_k^0 \mathbf{v}_h$ and $\Pi_k^0 \mathbf{w}_h$, which are computable from the degrees of freedom of \mathbf{v}_h and \mathbf{w}_h , respectively, see the previous section. The local form $S_m^P(\cdot, \cdot) : \mathbf{V}_k^h \times \mathbf{V}_k^h \rightarrow \mathbb{R}$ can be *any* symmetric and coercive bilinear form that is computable from the degrees of freedom and for which there exists two strictly positive real constants σ_* and σ^* such that

$$\sigma_* m^P(\mathbf{v}_h, \mathbf{v}_h) \leq S_m^P(\mathbf{v}_h, \mathbf{v}_h) \leq \sigma^* m^P(\mathbf{v}_h, \mathbf{v}_h) \quad \mathbf{v}_h \in \ker(\Pi_k^0) \cap \mathbf{V}_k^h(\mathbf{P}). \quad (25)$$

We can define computable stabilizations $S_m^P(\cdot, \cdot)$ by resorting to the two-dimensional implementations of the effective choices for the scalar case investigated in [64, 91]. The one used in our implementation of the method is discussed in subsection 3.5.

The discrete bilinear form $m_h^P(\cdot, \cdot)$ satisfies the two fundamental properties:

- *k*-consistency: for all $\mathbf{v}_h \in \mathbf{V}_k^h$ and for all $\mathbf{q} \in [\mathbb{P}_k(\mathbf{P})]^2$ it holds

$$m_h^P(\mathbf{v}_h, \mathbf{q}) = m^P(\mathbf{v}_h, \mathbf{q}); \quad (26)$$

- *stability*: there exists two positive constants μ_* , μ^* , independent of h , k and \mathbf{P} , such that

$$\mu_* m^P(\mathbf{v}_h, \mathbf{v}_h) \leq m_h^P(\mathbf{v}_h, \mathbf{v}_h) \leq \mu^* m^P(\mathbf{v}_h, \mathbf{v}_h) \quad \forall \mathbf{v}_h \in \mathbf{V}_k^h. \quad (27)$$

The local bilinear form a_h^P is given by

$$a_h^P(\mathbf{v}_h, \mathbf{w}_h) = \int_{\mathbf{P}} \mathrm{D}\Pi_{k-1}^0(\boldsymbol{\varepsilon}(\mathbf{v}_h)) : \Pi_{k-1}^0(\boldsymbol{\varepsilon}(\mathbf{w}_h)) \, dV + S_a^P(\mathbf{v}_h, \mathbf{w}_h), \quad (28)$$

where $S_a^P(\cdot, \cdot)$ is the local stabilization term. The bilinear form a_h^P depends on the orthogonal projections $\Pi_{k-1}^0 \nabla \mathbf{v}_h$ and $\Pi_{k-1}^0 \nabla \mathbf{w}_h$, which are computable from the degrees of freedom of \mathbf{v}_h and \mathbf{w}_h , respectively, see the previous section. $S_a^P(\cdot, \cdot) : \mathbf{V}_k^h \times \mathbf{V}_k^h \rightarrow \mathbb{R}$ and can be *any* symmetric and coercive bilinear form that is computable from the degrees of freedom and for which there exists two strictly positive real constants $\bar{\sigma}_*$ and $\bar{\sigma}^*$ such that

$$\bar{\sigma}_* a^P(\mathbf{v}_h, \mathbf{v}_h) \leq S_m^P(\mathbf{v}_h, \mathbf{v}_h) \leq \bar{\sigma}^* a^P(\mathbf{v}_h, \mathbf{v}_h) \quad \forall \mathbf{v}_h \in \ker(\Pi_k^0) \cap \mathbf{V}_k^h(\mathbf{P}). \quad (29)$$

Note that $S_a^P(\cdot, \cdot)$ must scale like $a^P(\cdot, \cdot)$, i.e., as $\mathcal{O}(1)$. We can define computable stabilizations $S_a^P(\cdot, \cdot)$ by resorting to the two-dimensional implementations of the effective choices for the scalar case investigated in [64, 91]. The one used in our implementations of the method is discussed in subsection 3.5.

The discrete bilinear form $a_h^P(\cdot, \cdot)$ satisfies the two fundamental properties:

- *k*-consistency: for all $\mathbf{v}_h \in \mathbf{V}_k^h$ and for all $\mathbf{q} \in [\mathbb{P}_k(\mathbf{P})]^2$ it holds

$$a_h^P(\mathbf{v}_h, \mathbf{q}) = a^P(\mathbf{v}_h, \mathbf{q}); \quad (30)$$

- *stability*: there exists two positive constants α_* , α^* , independent of h , k and \mathbf{P} , such that

$$\alpha_* a^P(\mathbf{v}_h, \mathbf{v}_h) \leq a_h^P(\mathbf{v}_h, \mathbf{v}_h) \leq \alpha^* a^P(\mathbf{v}_h, \mathbf{v}_h) \quad \forall \mathbf{v}_h \in \mathbf{V}_k^h. \quad (31)$$

Constants α_* and α^* may depend on μ and λ . See [28, Remark 6.1] for the independence of k .

Remark 3.3 We will use the stability of both $m_h^P(\cdot, \cdot)$ and $a_h^P(\cdot, \cdot)$ to prove that the semi-discrete virtual element approximation is stable in time, i.e., the approximate solution $\mathbf{u}_h(t)$ for all $t \in (0, T]$ depends continuously on the initial solutions \mathbf{u}_0 and the source term \mathbf{f} .

Remark 3.4 The stability of the symmetric bilinear forms $m_h^P(\cdot, \cdot)$ and $a_h^P(\cdot, \cdot)$ implies that both are inner products on \mathbf{V}_k^h , and, hence, that they are continuous. In fact, the Cauchy-Schwarz inequality and the local stability of m_h imply that

$$\begin{aligned} m_h(\mathbf{v}_h, \mathbf{w}_h) &\leq (m_h(\mathbf{v}_h, \mathbf{v}_h))^{\frac{1}{2}} (m_h(\mathbf{w}_h, \mathbf{w}_h))^{\frac{1}{2}} \leq \mu^* (m(\mathbf{v}_h, \mathbf{v}_h))^{\frac{1}{2}} (m(\mathbf{w}_h, \mathbf{w}_h))^{\frac{1}{2}} \\ &\leq \mu^* \|\rho\|_{\infty} \|\mathbf{v}_h\|_0 \|\mathbf{w}_h\|_0 \end{aligned} \quad (32)$$

for all $\mathbf{v}_h \in \mathbf{V}_k^h$. Similarly, the Cauchy-Schwarz inequality and the local stability of a_h imply that

$$a_h(\mathbf{v}_h, \mathbf{w}_h) \leq (a_h(\mathbf{v}_h, \mathbf{v}_h))^{\frac{1}{2}} (a_h(\mathbf{w}_h, \mathbf{w}_h))^{\frac{1}{2}} \leq \alpha^* (a(\mathbf{v}_h, \mathbf{v}_h))^{\frac{1}{2}} (a(\mathbf{w}_h, \mathbf{w}_h))^{\frac{1}{2}} = \alpha^* |\mathbf{v}_h|_{1,h} |\mathbf{w}_h|_{1,h} \quad (33)$$

for all $\mathbf{v}_h \in \mathbf{V}_k^h$.

3.4. Approximation of the right-hand side

We approximate the right-hand side (13) of the semi-discrete formulation (and, consequently, (14) of the full discrete formulation) as follows:

$$F_h(\mathbf{v}_h) = \int_{\Omega} \mathbf{f} \cdot \Pi_{k-2}^0(\mathbf{v}_h) \, dV + \sum_{e \in \Gamma_N} \int_{\Gamma_N} \mathbf{g}_N \cdot \Pi_k^{0,e}(\mathbf{v}_h) \quad \forall \mathbf{v}_h \in \mathbf{V}_k^h, \quad (34)$$

where $\Pi_k^{0,e}(\mathbf{v}_h)$ is the L^2 -orthogonal projection of the components of the virtual element vector field \mathbf{v}_h on the space of scalar polynomials defined on edge e . The linear functional $F_h(\cdot)$ is clearly computable since we have already noted that $\Pi_k^0(\mathbf{v}_h)$ and $\Pi_k^{0,e}(\mathbf{v}_h)$ are computable from the degrees of freedom of \mathbf{v}_h . Moreover, when $\mathbf{g}_N = 0$ using the stability of the projection operator and the Cauchy-Schwarz inequality, we note that

$$|F_h(\mathbf{v}_h)| \leq \left| \int_{\Omega} \mathbf{f}(t) \cdot \Pi_{k-2}^0(\mathbf{v}_h) dV \right| \leq \|\mathbf{f}(t)\|_0 \|\Pi_{k-2}^0(\mathbf{v}_h)\|_0 \leq \|\mathbf{f}(t)\|_0 \|\mathbf{v}_h\|_0 \quad \forall t \in [0, T]. \quad (35)$$

We will use (35) in the proof of the stability of the semi-discrete virtual element approximation.

3.5. The hitchiker's guide of the VEM for the elastodynamics

In this subsection, we present the implementation details that are practically useful and the basic steps to reduce the implementation of the VEM to the calculation of a few small elemental matrices. In fact, the implementation of the VEM relies on the L^2 -orthogonal projection matrices for scalar shape functions and their gradients. Their construction can be found, for example, in [22].

We build the mass and stiffness matrices of the VEM by applying definitions (24) and (28) to the vector-valued shape functions generating $\mathbf{V}_k^h(\mathbf{P})$. Let ϕ_i be the i -th “canonical” vector-valued basis function of the global virtual element space \mathbf{V}_k^h . We define the *mass matrix* $\mathbf{M} = (\mathbf{M}_{ij})$ and the *stiffness matrix* $\mathbf{K} = (\mathbf{K}_{ij})$ by $\mathbf{M}_{ij} = m_h(\phi_j, \phi_i)$ and $\mathbf{K}_{ij} = a_h(\phi_j, \phi_i)$, respectively. The stability condition (27) implies that $\|\phi_i\|_0^2 \lesssim m_h(\phi_i, \phi_i) \lesssim \|\phi_i\|_0^2$ for every i . Therefore, mass matrix \mathbf{M} is strictly positive definite (and symmetric) and, hence, nonsingular. Similarly, the stability condition (31) implies that $|\phi_i|_1^2 \lesssim a_h(\phi_i, \phi_i) \lesssim |\phi_i|_1^2$. Therefore, the stiffness matrix \mathbf{K} is non-negative definite (and symmetric).

As discussed in the previous subsections, the virtual element space of two-dimensional vector-valued functions $\mathbf{v}_h \in \mathbf{V}_k^h(\mathbf{P})$ is built by taking the two components of \mathbf{v}_h in the scalar virtual element space $V_k^h(\mathbf{P})$. Let ϕ_i be the shape function of $V_k^h(\mathbf{P})$ that is associated with the i -th degree of freedom, so that by definition, its i -th degree of freedom is equal to one, while all other degrees of freedom are equal to zero. Here, we consider the index i (and j in the next formulas) as running from 1 to N^{dofs} , where N^{dofs} is the dimension of $V_k^h(\mathbf{P})$. Using this convention, the dimension of the vector virtual element space $\mathbf{V}_k^h(\mathbf{P})$ is actually $2N^{\text{dofs}}$. Accordingly, the set of “canonical” shape functions that generate $\mathbf{V}_k^h(\mathbf{P})$ is given by vector-valued functions of the form $\phi_i^{\text{up}} = (\phi_i, 0)^T$ and $\phi_i^{\text{down}} = (0, \phi_i)^T$.

For the exposition's sake, we simplify the notation for the orthogonal projections. More precisely, we use the “hat” symbol over ϕ_i , e.g., $\hat{\phi}_i$, to denote the L^2 -projection of ϕ_i onto the polynomials of degree k . We also denote the partial derivatives of ϕ_i along the x and y direction by $\partial_x \phi_i$ and $\partial_y \phi_i$, respectively, and, with a small abuse of notation, their L^2 -orthogonal projections onto the polynomials of degree $k-1$ by $\widehat{\partial}_x \phi_i$ and $\widehat{\partial}_y \phi_i$. As discussed previously, all these projections are computable from the degrees of freedom of ϕ_i , cf. [22, 55].

Let $\mathbf{M} = \mathbf{M}^c + \mathbf{M}^s$ and $\mathbf{K} = \mathbf{K}^c + \mathbf{K}^s$ be the mass and stiffness matrices, that we write as the sum of the consistence term, i.e., matrices \mathbf{M}^c and \mathbf{K}^c , and stability term, i.e., matrices \mathbf{M}^s and \mathbf{K}^s . In the rest of this section, we detail the construction of each one of these four matrix terms.

The splitting of the polygonal shape functions in vector-valued functions like ϕ_i^{up} and ϕ_i^{down} , where only one components is actually nonzero, simplifies the expression of the mass matrix significantly. Matrix \mathbf{M}^c is, indeed, block diagonal, each block has size $N^{\text{dofs}} \times N^{\text{dofs}}$, and its (ij) -th entry is given by

$$\mathbf{M}_{ij}^c = \int_{\mathbf{P}} \hat{\phi}_i \hat{\phi}_j dV. \quad (36)$$

Let $\mathbf{\Pi}_k^0$ be the projection matrix of the set of scalar shape functions $\{\phi_i\}_{i=1}^{N^{\text{dofs}}}$. Matrix $\mathbf{\Pi}_k^0$ has size $N^k \times N^{\text{dofs}}$, where N^k is the dimension of $\mathbb{P}_k(\mathbf{P})$. The coefficients of the expansion of ϕ_i on the monomial basis are on the i -th columns of $\mathbf{\Pi}_k^0$, so that:

$$\hat{\phi}_i(x, y) = \sum_{\alpha=1}^{N^k} m_{\alpha}(x, y) (\mathbf{\Pi}_k^0)_{\alpha, i}. \quad (37)$$

Using this polynomial expansion we find that

$$\mathbf{M}_{ij}^c = \sum_{\alpha, \beta=1}^{N^k} \mathbf{Q}_{\alpha, \beta} (\boldsymbol{\Pi}_k^0)_{\alpha, i} (\boldsymbol{\Pi}_k^0)_{\beta, j}, \quad (38)$$

where \mathbf{Q} is the mass matrix of the monomials,

$$\mathbf{Q}_{\alpha, \beta} = \int_{\mathbf{P}} m_{\beta}(x, y) m_{\alpha}(x, y) dV. \quad (39)$$

The equivalent matrix form is

$$\mathbf{M}^c = (\boldsymbol{\Pi}_k^0)^T \mathbf{Q} \boldsymbol{\Pi}_k^0. \quad (40)$$

The stability matrix used in this work is obtained from the stabilization bilinear form

$$S_m^P(\mathbf{v}_h, \mathbf{w}_h) = \bar{\rho} h_{\mathbf{P}}^2 \sum_{\ell=1}^{2N^{\text{dofs}}} \text{dof}_{\ell}(\mathbf{v}_h) \text{dof}_{\ell}(\mathbf{w}_h), \quad (41)$$

where $\bar{\rho}$ is the cell-average of ρ over \mathbf{P} . We recall that ℓ runs from 1 to $2N^{\text{dofs}}$ since N^{dofs} is the number of degrees of freedom of the scalar virtual element space. Using $\phi_i^{\text{up}} = (\phi_i, 0)^T$ and $\phi_i^{\text{down}} = (0, \phi_i)^T$ for the vector basis functions, the stability part of the mass matrix is provided by the formula:

$$\begin{aligned} \mathbf{M}_{ij}^s = \bar{\rho} h_{\mathbf{P}}^2 \sum_{\ell=1}^{2N^{\text{dofs}}} & \left[\text{dof}_{\ell}((1 - \boldsymbol{\Pi}_k^0) \phi_i^{\text{up}}) \text{dof}_{\ell}((1 - \boldsymbol{\Pi}_k^0) \phi_j^{\text{up}}) \right. \\ & \left. + \text{dof}_{\ell}((1 - \boldsymbol{\Pi}_k^0) \phi_i^{\text{down}}) \text{dof}_{\ell}((1 - \boldsymbol{\Pi}_k^0) \phi_j^{\text{down}}) \right] \end{aligned} \quad (42)$$

Using $\phi_i^{\text{up}} = (\phi_i, 0)^T$ and $\phi_i^{\text{down}} = (0, \phi_i)^T$ for the vector basis functions, the stability part of the mass matrix is provided by the formula:

$$\mathbf{M}_{ij}^s = \bar{\rho} h_{\mathbf{P}}^2 \begin{bmatrix} (\mathbf{I} - \boldsymbol{\Pi}_k^0)^T (\mathbf{I} - \boldsymbol{\Pi}_k^0) & 0 \\ 0 & (\mathbf{I} - \boldsymbol{\Pi}_k^0)^T (\mathbf{I} - \boldsymbol{\Pi}_k^0) \end{bmatrix}. \quad (43)$$

The block-diagonal structure above is induced by our choice of using the vector basis functions $\phi_i^{\text{up}} = (\phi_i, 0)^T$ and $\phi_i^{\text{down}} = (0, \phi_i)^T$.

The situation is more complex for the stiffness matrix, where the splitting “up – down” induces the 2×2 splitting:

$$\mathbf{K}^c = \begin{bmatrix} \mathbf{K}^{c, \text{up,up}} & \mathbf{K}^{c, \text{up,down}} \\ \mathbf{K}^{c, \text{down,up}} & \mathbf{K}^{c, \text{down,down}} \end{bmatrix}. \quad (44)$$

To detail each one of these four submatrices, consider first a generic vector-valued field $\mathbf{w} = (w_x, w_y)^T$. From the standard definition of the tensor fields $\boldsymbol{\varepsilon}(\mathbf{w})$ and $\boldsymbol{\sigma}(\mathbf{w})$, we immediately find that:

$$\boldsymbol{\varepsilon}(\mathbf{w}) = \begin{bmatrix} \partial_x w_x & \frac{1}{2}(\partial_x w_y + \partial_y w_x) \\ \frac{1}{2}(\partial_x w_y + \partial_y w_x) & \partial_y w_y \end{bmatrix} \quad (45)$$

and, according to (8),

$$\boldsymbol{\sigma}(\mathbf{w}) = \begin{bmatrix} (2\mu + \lambda) \partial_x w_x + \lambda \partial_y w_y & \mu(\partial_x w_y + \partial_y w_x) \\ \mu(\partial_x w_y + \partial_y w_x) & \lambda \partial_x w_x + (2\mu + \lambda) \partial_y w_y \end{bmatrix}. \quad (46)$$

Then, we take $\mathbf{w} \in \{\phi_i^{\text{up}}, \phi_i^{\text{down}}\}_{i=1}^{N^{\text{dofs}}}$, so that

$$\boldsymbol{\varepsilon}(\phi_i^{\text{up}}) = \begin{bmatrix} \partial_x \phi_i & \frac{1}{2} \partial_y \phi_i \\ \frac{1}{2} \partial_y \phi_i & 0 \end{bmatrix}, \quad \boldsymbol{\varepsilon}(\phi_i^{\text{down}}) = \begin{bmatrix} 0 & \frac{1}{2} \partial_x \phi_i \\ \frac{1}{2} \partial_x \phi_i & \partial_y \phi_i \end{bmatrix} \quad (47)$$

and

$$\boldsymbol{\sigma}(\phi_i^{\text{up}}) = \begin{bmatrix} (2\mu + \lambda) \partial_x \phi_i & \mu \partial_y \phi_i \\ \mu \partial_y \phi_i & \lambda \partial_x \phi_i \end{bmatrix}, \quad \boldsymbol{\sigma}(\phi_i^{\text{down}}) = \begin{bmatrix} \lambda \partial_y \phi_i & \mu \partial_x \phi_i \\ \mu \partial_x \phi_i & (2\mu + \lambda) \partial_y \phi_i \end{bmatrix}. \quad (48)$$

Using such definitions, a straightforward calculation immediately provides us the formulas for the stiffness submatrices:

$$\begin{aligned} \mathbf{K}_{ij}^{c,\text{up,up}} &= \int_{\mathbf{P}} \widehat{\boldsymbol{\sigma}(\phi_j^{\text{up}})} : \widehat{\boldsymbol{\varepsilon}(\phi_i^{\text{up}})} \, dV = (2\mu + \lambda) \int_{\mathbf{P}} \widehat{\partial_x \phi_j} \widehat{\partial_x \phi_i} \, dV + \mu \int_{\mathbf{P}} \widehat{\partial_y \phi_j} \widehat{\partial_y \phi_i} \, dV, \\ \mathbf{K}_{ij}^{c,\text{up,down}} &= \int_{\mathbf{P}} \widehat{\boldsymbol{\sigma}(\phi_j^{\text{up}})} : \widehat{\boldsymbol{\varepsilon}(\phi_i^{\text{down}})} \, dV = \mu \int_{\mathbf{P}} \widehat{\partial_y \phi_j} \widehat{\partial_x \phi_i} \, dV + \lambda \int_{\mathbf{P}} \widehat{\partial_x \phi_j} \widehat{\partial_y \phi_i} \, dV, \\ \mathbf{K}_{ij}^{c,\text{down,up}} &= \int_{\mathbf{P}} \widehat{\boldsymbol{\sigma}(\phi_j^{\text{down}})} : \widehat{\boldsymbol{\varepsilon}(\phi_i^{\text{up}})} \, dV = \lambda \int_{\mathbf{P}} \widehat{\partial_y \phi_j} \widehat{\partial_x \phi_i} \, dV + \mu \int_{\mathbf{P}} \widehat{\partial_x \phi_j} \widehat{\partial_y \phi_i} \, dV, \\ \mathbf{K}_{ij}^{c,\text{down,down}} &= \int_{\mathbf{P}} \widehat{\boldsymbol{\sigma}(\phi_j^{\text{down}})} : \widehat{\boldsymbol{\varepsilon}(\phi_i^{\text{down}})} \, dV = \mu \int_{\mathbf{P}} \widehat{\partial_x \phi_j} \widehat{\partial_x \phi_i} \, dV + (2\mu + \lambda) \int_{\mathbf{P}} \widehat{\partial_y \phi_j} \widehat{\partial_y \phi_i} \, dV. \end{aligned} \quad (49)$$

A thorough inspection of these formulas reveals that we only need the two projection matrices $\boldsymbol{\Pi}_{k-1}^{0,x}$ and $\boldsymbol{\Pi}_{k-1}^{0,y}$ such that

$$\widehat{\partial_x \phi_i}(x, y) = \sum_{\alpha=1}^{N^{k-1}} m_{\alpha}(x, y) (\boldsymbol{\Pi}_{k-1}^{0,x})_{\alpha,i}, \quad \widehat{\partial_y \phi_i}(x, y) = \sum_{\alpha=1}^{N^{k-1}} m_{\alpha}(x, y) (\boldsymbol{\Pi}_{k-1}^{0,y})_{\alpha,i}, \quad (50)$$

and the four additional matrices involving the derivatives of monomials up to the degree k :

$$\begin{aligned} \mathbf{Q}_{\alpha,\beta}^{xx} &= \int_{\mathbf{P}} \partial_x m_{\beta} \partial_x m_{\alpha} \, dV, & \mathbf{Q}_{\alpha,\beta}^{xy} &= \int_{\mathbf{P}} \partial_x m_{\beta} \partial_y m_{\alpha} \, dV, \\ \mathbf{Q}_{\alpha,\beta}^{yx} &= \int_{\mathbf{P}} \partial_y m_{\beta} \partial_x m_{\alpha} \, dV, & \mathbf{Q}_{\alpha,\beta}^{yy} &= \int_{\mathbf{P}} \partial_y m_{\beta} \partial_y m_{\alpha} \, dV. \end{aligned}$$

Using such matrices we can reformulate the entries of the four subblocks of matrix \mathbf{K}^c as follows:

$$\begin{aligned} \mathbf{K}_{ij}^{c,\text{up,up}} &= (2\mu + \lambda) \sum_{\alpha,\beta} \mathbf{Q}_{\alpha,\beta}^{xx} (\boldsymbol{\Pi}_{k-1}^{0,x})_{\alpha,i} (\boldsymbol{\Pi}_{k-1}^{0,x})_{\beta,j} + \mu \sum_{\alpha,\beta} \mathbf{Q}_{\alpha,\beta}^{yx} (\boldsymbol{\Pi}_{k-1}^{0,y})_{\alpha,i} (\boldsymbol{\Pi}_{k-1}^{0,y})_{\beta,j}, \\ \mathbf{K}_{ij}^{c,\text{up,down}} &= \mu \sum_{\alpha,\beta} \mathbf{Q}_{\alpha,\beta}^{xy} (\boldsymbol{\Pi}_{k-1}^{0,x})_{\alpha,i} (\boldsymbol{\Pi}_{k-1}^{0,y})_{\beta,j} + \lambda \sum_{\alpha,\beta} \mathbf{Q}_{\alpha,\beta}^{yx} (\boldsymbol{\Pi}_{k-1}^{0,y})_{\alpha,i} (\boldsymbol{\Pi}_{k-1}^{0,x})_{\beta,j}, \\ \mathbf{K}_{ij}^{c,\text{down,up}} &= \lambda \sum_{\alpha,\beta} \mathbf{Q}_{\alpha,\beta}^{xy} (\boldsymbol{\Pi}_{k-1}^{0,x})_{\alpha,i} (\boldsymbol{\Pi}_{k-1}^{0,y})_{\beta,j} + \mu \sum_{\alpha,\beta} \mathbf{Q}_{\alpha,\beta}^{yy} (\boldsymbol{\Pi}_{k-1}^{0,y})_{\alpha,i} (\boldsymbol{\Pi}_{k-1}^{0,x})_{\beta,j}, \\ \mathbf{K}_{ij}^{c,\text{down,down}} &= \mu \sum_{\alpha,\beta} \mathbf{Q}_{\alpha,\beta}^{xx} (\boldsymbol{\Pi}_{k-1}^{0,x})_{\alpha,i} (\boldsymbol{\Pi}_{k-1}^{0,x})_{\beta,j} + (2\mu + \lambda) \sum_{\alpha,\beta} \mathbf{Q}_{\alpha,\beta}^{yy} (\boldsymbol{\Pi}_{k-1}^{0,y})_{\alpha,i} (\boldsymbol{\Pi}_{k-1}^{0,y})_{\beta,j}. \end{aligned} \quad (51)$$

The equivalent compact matrix form is:

$$\begin{aligned}
\mathbf{K}^{c,\text{up,up}} &= (2\mu + \lambda)(\boldsymbol{\Pi}_{k-1}^{0,x})^T \mathbf{Q}^{xx} \boldsymbol{\Pi}_{k-1}^{0,x} + \mu(\boldsymbol{\Pi}_{k-1}^{0,y})^T \mathbf{Q}^{yy} \boldsymbol{\Pi}_{k-1}^{0,y}, \\
\mathbf{K}^{c,\text{up,down}} &= \mu(\boldsymbol{\Pi}_{k-1}^{0,x})^T \mathbf{Q}^{xy} \boldsymbol{\Pi}_{k-1}^{0,y} + \lambda(\boldsymbol{\Pi}_{k-1}^{0,y})^T \mathbf{Q}^{yx} \boldsymbol{\Pi}_{k-1}^{0,x}, \\
\mathbf{K}^{c,\text{down,up}} &= \lambda(\boldsymbol{\Pi}_{k-1}^{0,x})^T \mathbf{Q}^{xy} \boldsymbol{\Pi}_{k-1}^{0,y} + \mu(\boldsymbol{\Pi}_{k-1}^{0,y})^T \mathbf{Q}^{yx} \boldsymbol{\Pi}_{k-1}^{0,x}, \\
\mathbf{K}^{c,\text{down,down}} &= \mu(\boldsymbol{\Pi}_{k-1}^{0,x})^T \mathbf{Q}^{xx} \boldsymbol{\Pi}_{k-1}^{0,x} + (2\mu + \lambda)(\boldsymbol{\Pi}_{k-1}^{0,y})^T \mathbf{Q}^{yy} \boldsymbol{\Pi}_{k-1}^{0,y}.
\end{aligned} \tag{52}$$

The stability matrix used in this work is obtained from the stabilization bilinear form

$$S_a^P(\mathbf{v}_h, \mathbf{w}_h) = \max(2\bar{\mu}, \bar{\lambda}) \sum_{\ell=1}^{2N^{\text{dofs}}} \text{dof}_\ell(\mathbf{v}_h) \text{dof}_\ell(\mathbf{w}_h), \tag{53}$$

where $\bar{\mu}$ and $\bar{\lambda}$ are the cell averages of μ and λ , respectively. Since we assume that the Lamé coefficients are constant, $\bar{\mu}$ and $\bar{\lambda}$ are respectively equal to μ and λ . We recall that index ℓ runs from 1 to $2N^{\text{dofs}}$ because N^{dofs} is the number of degrees of freedom of the scalar virtual element space. Using $\phi_i^{\text{up}} = (\phi_i, 0)^T$ and $\phi_i^{\text{down}} = (0, \phi_i)^T$ for the vector basis functions, the stability part of the mass matrix is provided by the formula:

$$\begin{aligned}
\mathbf{K}_{ij}^s &= \max(2\bar{\mu}, \bar{\lambda}) \sum_{\ell=1}^{N^{\text{dofs}}} \left[\text{dof}_\ell \left(\left(1 - \Pi_k^{\nabla, P} \right) \phi_i^{\text{up}} \right) \text{dof}_\ell \left(\left(1 - \Pi_k^{\nabla, P} \right) \phi_j^{\text{up}} \right) \right. \\
&\quad \left. + \text{dof}_\ell \left(\left(1 - \Pi_k^{\nabla, P} \right) \phi_i^{\text{down}} \right) \text{dof}_\ell \left(\left(1 - \Pi_k^{\nabla, P} \right) \phi_j^{\text{down}} \right) \right].
\end{aligned} \tag{54}$$

The stability matrix can be written in block-diagonal form, and in this work we consider

$$\mathbf{K}^s = \max(2\bar{\mu}, \bar{\lambda}) \begin{bmatrix} (\mathbf{I} - \boldsymbol{\Pi}_k^{\nabla})^T (\mathbf{I} - \boldsymbol{\Pi}_k^{\nabla}) & 0 \\ 0 & (\mathbf{I} - \boldsymbol{\Pi}_k^{\nabla})^T (\mathbf{I} - \boldsymbol{\Pi}_k^{\nabla}) \end{bmatrix}, \tag{55}$$

where $\boldsymbol{\Pi}_k^{\nabla}$ is the elliptic projection matrix for the scalar case. An alternative formulation can be obtained by considering the orthogonal projector $\boldsymbol{\Pi}_k^{0,P}$ instead of the elliptic projector $\boldsymbol{\Pi}_k^{\nabla,P}$ in (54), and, consistently, the orthogonal projection matrix $\boldsymbol{\Pi}_k^0$ instead of $\boldsymbol{\Pi}_k^{\nabla}$ in (55).

4. Stability and convergence analysis for the semi-discrete problem

The main results of this section are stated in Theorems 4.5, 4.6 and 4.8, which respectively prove the stability and convergence in the mesh dependent energy norm that will be introduced in (58) and the convergence in the $L^2(\Omega)$ -norm. For exposition's sake, we set $\rho = 1$ in (3), (9) and (24) and $\mathbf{g}_N = 0$ in (5), (11) and (34).

4.1. Technicalities and preliminary results

To carry out the analysis of this section and derive *a priori* estimates, we need the error estimates for piecewise polynomial approximations and interpolation in the virtual element space \mathbf{V}_k^h that are stated in the two following lemmas.

Lemma 4.1 *Let $\mathbb{P}_k(\Omega_h)$ be the space of discontinuous polynomials of degree up to k defined on mesh Ω_h . Under the mesh regularity assumption **(A0)**, for all $\mathbf{u} \in H^{m+1}(\Omega)$, $m \in \mathbb{N}$, there exists a vector-valued field $\mathbf{u}_\pi \in [\mathbb{P}_k(\Omega_h)]^2$ such that*

$$\begin{aligned}\|\mathbf{u} - \mathbf{u}_\pi\|_0 &\lesssim \frac{h^{\mu+1}}{k^{m+1}} \|\mathbf{u}\|_{m+1} \quad \mu = \min(k, m), m \geq 0, \\ |\mathbf{u} - \mathbf{u}_\pi|_{1,h} &\lesssim \frac{h^\mu}{k^m} \|\mathbf{u}\|_{m+1} \quad \mu = \min(k, m), m \geq 1.\end{aligned}\tag{56}$$

Proof. The assertion of the lemma is proved in [28]. \square

Lemma 4.2 *Under the mesh regularity assumption (A0), for all $\mathbf{u} \in H^{m+1}(\Omega)$, $m \in \mathbb{N}$, there exists a virtual element interpolant $\mathbf{u}_I \in \mathbf{V}_k^h$ such that*

$$\begin{aligned}\|\mathbf{u} - \mathbf{u}_I\|_0 &\lesssim \frac{h^{\mu+1}}{k^m} \|\mathbf{u}\|_{m+1} \quad \mu = \min(k, m), m \geq 0 \\ |\mathbf{u} - \mathbf{u}_I|_1 &\lesssim \frac{h^\mu}{k^m} \|\mathbf{u}\|_{m+1} \quad \mu = \min(k, m), m \geq 1.\end{aligned}\tag{57}$$

Proof. The assertion of the lemma is proved in [57]. \square

Remark 4.3 *The L^2 -estimate provided by Lemma 4.2 is suboptimal in k as we have a dependence like k^m instead of k^{m+1} in the fraction denominators. Nonetheless, as observed in [28], whenever the components of \mathbf{u} are the restrictions to Ω of analytic functions, it is still possible prove that the rate of convergence in terms of m is exponential.*

4.2. Stability

The semi-discrete virtual element approximation of the time-dependent linear elastodynamics problem in variational form is stable and convergent, cf. Theorems 4.5 and 4.6 below, which are the main results of this section. Moreover, we state Theorems 4.5 and 4.6 below by using the *energy norm*

$$\|\mathbf{v}_h(t)\|^2 = \left\| \rho^{\frac{1}{2}} \dot{\mathbf{v}}_h(t) \right\|_0^2 + |\mathbf{v}_h(t)|_1^2, \quad t \in [0, T],\tag{58}$$

which is defined for all $v \in \mathbf{V}_k^h$. The local stability property of the bilinear forms $m_h(\cdot, \cdot)$ and $a_h(\cdot, \cdot)$ readily imply the equivalence relation

$$m_h(\dot{\mathbf{v}}_h, \dot{\mathbf{v}}_h) + a_h(\mathbf{v}_h, \mathbf{v}_h) \lesssim \|\mathbf{v}_h(t)\|^2 \lesssim m_h(\dot{\mathbf{v}}_h, \dot{\mathbf{v}}_h) + a_h(\mathbf{v}_h, \mathbf{v}_h)\tag{59}$$

for all time-dependent virtual element functions $\mathbf{v}_h(t)$ with square integrable derivative $\dot{\mathbf{v}}_h(t)$.

Remark 4.4 *The hidden constants in (59) may depend on the stability parameters μ_* , μ^* , α_* , α^* , the regularity constant ϱ of the mesh, and the polynomial degree k (see [28, Remark 6.1] for more details). However, they are independent of the mesh size parameter h .*

Theorem 4.5 *Let $\mathbf{f} \in L^2((0, T]; [L^2(\Omega)]^2)$ and let $\mathbf{u}_h \in C^2((0, T]; \mathbf{V}_k^h)$ be the solution of (13). Then, it holds*

$$\|\mathbf{u}_h(t)\| \lesssim \|(\mathbf{u}_0)_I\| + \int_0^t \|\mathbf{f}(\tau)\|_{0,\Omega} d\tau.\tag{60}$$

Proof. We substitute $\mathbf{v}_h = \dot{\mathbf{u}}_h(t)$ in (13) and, for all $t \in (0, T]$, we obtain

$$m_h(\ddot{\mathbf{u}}_h, \dot{\mathbf{u}}_h) + a_h(\mathbf{u}_h, \dot{\mathbf{u}}_h) = F_h(\dot{\mathbf{u}}_h).\tag{61}$$

Since both $m_h(\cdot, \cdot)$ and $a_h(\cdot, \cdot)$ are symmetric bilinear forms, a straightforward calculation yields

$$\frac{1}{2} \frac{d}{dt} (m_h(\dot{\mathbf{u}}_h, \dot{\mathbf{u}}_h) + a_h(\mathbf{u}_h, \dot{\mathbf{u}}_h)) = m_h(\ddot{\mathbf{u}}_h, \dot{\mathbf{u}}_h) + a_h(\mathbf{u}_h, \dot{\mathbf{u}}_h).$$

We substitute this expression in the left-hand side of (61), we integrate in time the resulting equation from 0 to the intermediate time t , and using the definition of norm $\|\cdot\|$ in (58) and the equivalence relation (59), we find that

$$\begin{aligned}
\|\|\mathbf{u}_h(t)\|\|^2 &\lesssim m_h(\dot{\mathbf{u}}_h(t), \dot{\mathbf{u}}_h(t)) + a_h(\mathbf{u}_h(t), \mathbf{u}_h(t)) \\
&= m_h(\dot{\mathbf{u}}_h(0), \dot{\mathbf{u}}_h(0)) + a_h(\mathbf{u}_h(0), \mathbf{u}_h(0)) + 2 \int_0^t F_h(\dot{\mathbf{u}}_h(\tau)) d\tau \\
&\lesssim \|\|\mathbf{u}_h(0)\|\|^2 + \int_0^t F_h(\dot{\mathbf{u}}_h(\tau)) d\tau.
\end{aligned}$$

Since $\mathbf{u}_h(0) = (\mathbf{u}_0)_I$, and using (35) (with $\mathbf{v}_h = \dot{\mathbf{u}}_h$), we find that

$$\|\|\mathbf{u}_h(t)\|\|^2 \lesssim \|(\mathbf{u}_0)_I\|^2 + \int_0^t F_h(\dot{\mathbf{u}}_h(\tau)) d\tau \lesssim \|(\mathbf{u}_0)_I\|^2 + \int_0^t \|\mathbf{f}(\tau)\|_0 \|\dot{\mathbf{u}}_h(\tau)\|_0 d\tau.$$

The thesis follows on applying [47, Lemma A5, p. 157]. \square

4.3. Convergence analysis in the energy norm

In this section, we prove the convergence of the semi-discrete virtual element approximation in the energy norm (58). *A priori* error estimates of the approximation error are derived from Theorem 4.6 as a corollary, which is reported at the end of the section, by using approximation results for discontinuous polynomial and virtual element spaces.

Theorem 4.6 *Let $\mathbf{u} \in C^2((0, T]; [H^{m+1}(\Omega)]^2)$, $m \in \mathbb{N}$, be the exact solution of problem (12). Let $\mathbf{u}_h \in \mathbf{V}_k^h$ be the solution of the semi-discrete problem (13) under the mesh regularity assumption (A0). Then, for all $t \in [0, T]$ and all discontinuous polynomial approximations $\mathbf{u}_\pi(t)$ of $\mathbf{u}(t)$, it holds that*

$$\|\|\mathbf{u}(t) - \mathbf{u}_h(t)\|\| \lesssim \sup_{\tau \in [0, T]} G_0(\tau) + \int_0^t G_1(\tau) d\tau, \quad (62)$$

where

$$G_0(\tau) = \|\dot{\mathbf{u}}(\tau) - \dot{\mathbf{u}}_I(\tau)\|_0 + |\mathbf{u}(\tau) - \mathbf{u}_I(\tau)|_1 + |\mathbf{u}(\tau) - \mathbf{u}_\pi(\tau)|_1, \quad (63)$$

$$\begin{aligned}
G_1(\tau) &= \|\ddot{\mathbf{u}}(\tau) - \ddot{\mathbf{u}}_I(\tau)\|_0 + \|\ddot{\mathbf{u}}(\tau) - \ddot{\mathbf{u}}_\pi(\tau)\|_0 + |\dot{\mathbf{u}}(\tau) - \dot{\mathbf{u}}_I(\tau)|_1 + |\dot{\mathbf{u}}(\tau) - \dot{\mathbf{u}}_\pi(\tau)|_1 \\
&\quad + \sup_{\mathbf{v}_h \in \mathbf{V}_k^h} \frac{|F(\mathbf{v}_h) - F_h(\mathbf{v}_h)|}{|\mathbf{v}_h|_1}.
\end{aligned} \quad (64)$$

Proof. Since \mathbf{V}_k^h is a subspace of \mathbf{V} , we can take $\mathbf{v}_h \in \mathbf{V}_k^h$ as test function in (12) and subtract from (13) to find the error equation:

$$m(\ddot{\mathbf{u}}(t), \mathbf{v}_h) - m_h(\ddot{\mathbf{u}}_h(t), \mathbf{v}_h) + a(\mathbf{u}(t), \mathbf{v}_h) - a_h(\mathbf{u}_h(t), \mathbf{v}_h) = F(\mathbf{v}_h) - F_h(\mathbf{v}_h), \quad (65)$$

which holds for all $\mathbf{v}_h \in \mathbf{V}_k^h$. Next, we rewrite this equation as $\mathbf{T}_1 + \mathbf{T}_2 = \mathbf{T}_3$, with the definitions:

$$\mathbf{T}_1 := m(\ddot{\mathbf{u}}, \mathbf{v}_h) - m_h(\ddot{\mathbf{u}}_h, \mathbf{v}_h),$$

$$\mathbf{T}_2 := a(\mathbf{u}, \mathbf{v}_h) - a_h(\mathbf{u}_h, \mathbf{v}_h),$$

$$\mathbf{T}_3 := F(\mathbf{v}_h) - F_h(\mathbf{v}_h),$$

where we dropped out the explicit dependence on t to simplify the notation. We analyze each term separately. First, we rewrite \mathbf{T}_1 as

$$\mathbf{T}_1 = m_h(\ddot{\mathbf{u}}_I - \ddot{\mathbf{u}}_h, \mathbf{v}_h) + m(\ddot{\mathbf{u}} - \ddot{\mathbf{u}}_\pi, \mathbf{v}_h) - m_h(\ddot{\mathbf{u}}_I - \ddot{\mathbf{u}}_\pi, \mathbf{v}_h)$$

by adding and subtracting $\ddot{\mathbf{u}}_I$ and $\ddot{\mathbf{u}}_\pi$ to the arguments of $m(\cdot, \cdot)$ and $m_h(\cdot, \cdot)$ and noting that $m(\ddot{\mathbf{u}}_\pi, \mathbf{v}_h) = m_h(\ddot{\mathbf{u}}_\pi, \mathbf{v}_h)$ for all $\mathbf{v}_h \in \mathbf{V}_k^h$. We also rewrite \mathbf{T}_2 as

$$\mathbf{T}_2 = a_h(\mathbf{u}_I - \mathbf{u}_h, \mathbf{v}_h) + a(\mathbf{u} - \mathbf{u}_\pi, \mathbf{v}_h) - a_h(\mathbf{u}_I - \mathbf{u}_\pi, \mathbf{v}_h)$$

by adding and subtracting \mathbf{u}_I and \mathbf{u}_π to the arguments of $a(\cdot, \cdot)$ and $a_h(\cdot, \cdot)$ and noting that $a(\mathbf{u}_\pi, \mathbf{v}_h) = a_h(\mathbf{u}_\pi, \mathbf{v}_h)$ for all $\mathbf{v}_h \in \mathbf{V}_k^h$. Let $\mathbf{e}_h = \mathbf{u}_I - \mathbf{u}_h$. It holds that $\mathbf{e}_h(0) = \dot{\mathbf{e}}_h(0) = 0$ since $\mathbf{u}_h(0) = (\mathbf{u}_0(0))_I = \mathbf{u}_I(0)$ and $\dot{\mathbf{u}}_h(0) = (\mathbf{u}_1(0))_I = \dot{\mathbf{u}}_I(0)$. Then, using the definition of \mathbf{e}_h , we reconsider the error equation

$$\begin{aligned} \mathsf{T}_1 + \mathsf{T}_2 &= m_h(\ddot{\mathbf{e}}_h, \mathbf{v}_h) + a_h(\mathbf{e}_h, \mathbf{v}_h) + m(\ddot{\mathbf{u}} - \ddot{\mathbf{u}}_\pi, \mathbf{v}_h) - m_h(\ddot{\mathbf{u}}_I - \ddot{\mathbf{u}}_\pi, \mathbf{v}_h) \\ &\quad + a(\mathbf{u} - \mathbf{u}_\pi, \mathbf{v}_h) - a_h(\mathbf{u}_I - \mathbf{u}_\pi, \mathbf{v}_h) = F(\mathbf{v}_h) - F_h(\mathbf{v}_h). \end{aligned} \quad (66)$$

Assume that $\mathbf{v}_h \neq 0$ and consider the inequalities:

$$|F(\mathbf{v}_h) - F_h(\mathbf{v}_h)| = \frac{|F(\mathbf{v}_h) - F_h(\mathbf{v}_h)|}{|\mathbf{v}_h|_1} |\mathbf{v}_h|_1 \leq \left(\sup_{\mathbf{v}_h \in \mathbf{V}_k^h \setminus \{0\}} \frac{|F(\mathbf{v}_h) - F_h(\mathbf{v}_h)|}{|\mathbf{v}_h|_1} \right) |\mathbf{v}_h|_1. \quad (67)$$

Note that there hold:

$$m_h(\ddot{\mathbf{e}}_h, \dot{\mathbf{e}}_h) + a_h(\mathbf{e}_h, \dot{\mathbf{e}}_h) = \frac{1}{2} \frac{d}{dt} (m_h(\dot{\mathbf{e}}_h, \dot{\mathbf{e}}_h) + a_h(\mathbf{e}_h, \mathbf{e}_h)), \quad (68)$$

$$|F(\dot{\mathbf{e}}_h) - F_h(\dot{\mathbf{e}}_h)| \leq \left(\sup_{\mathbf{v}_h \in \mathbf{V}_k^h \setminus \{0\}} \frac{|F(\mathbf{v}_h) - F_h(\mathbf{v}_h)|}{|\mathbf{v}_h|_1} \right) \|\mathbf{e}_h\|. \quad (69)$$

Setting $\mathbf{v}_h = \dot{\mathbf{e}}_h(t)$ on the left-hand side of (66) and employing (68)-(69) together with (65), we obtain, after rearranging the terms, that:

$$\begin{aligned} \frac{1}{2} \frac{d}{dt} (m_h(\dot{\mathbf{e}}_h, \dot{\mathbf{e}}_h) + a_h(\mathbf{e}_h, \mathbf{e}_h)) &\leq -m(\ddot{\mathbf{u}} - \ddot{\mathbf{u}}_\pi, \dot{\mathbf{e}}_h) + m_h(\ddot{\mathbf{u}}_I - \ddot{\mathbf{u}}_\pi, \dot{\mathbf{e}}_h) \\ &\quad - a(\mathbf{u} - \mathbf{u}_\pi, \dot{\mathbf{e}}_h) + a_h(\mathbf{u}_I - \mathbf{u}_\pi, \dot{\mathbf{e}}_h) \\ &\quad + \left(\sup_{\mathbf{v}_h \in \mathbf{V}_k^h \setminus \{0\}} \frac{|F(\mathbf{v}_h) - F_h(\mathbf{v}_h)|}{|\mathbf{v}_h|_1} \right) \|\mathbf{e}_h\|. \end{aligned} \quad (70)$$

To ease the notation, we collect together the last two terms above and denote them by $\mathsf{R}_1(t)$ (note that they still depend on t). We integrate in time from 0 to t both sides of (70), note that the initial term is zero since $\mathbf{e}_h(0) = \dot{\mathbf{e}}_h(0) = 0$ and use (59)

$$\begin{aligned} \|\mathbf{e}_h(t)\|^2 &\leq m_h(\dot{\mathbf{e}}_h(t), \dot{\mathbf{e}}_h(t)) + a_h(\mathbf{e}_h(t), \mathbf{e}_h(t)) \\ &\leq \int_0^t \left(\mathsf{R}_1(\tau) - m(\ddot{\mathbf{u}}(\tau) - \ddot{\mathbf{u}}_\pi(\tau), \dot{\mathbf{e}}_h(\tau)) + m_h(\ddot{\mathbf{u}}_I(\tau) - \ddot{\mathbf{u}}_\pi(\tau), \dot{\mathbf{e}}_h(\tau)) \right. \\ &\quad \left. - a(\mathbf{u}(\tau) - \mathbf{u}_\pi(\tau), \dot{\mathbf{e}}_h(\tau)) + a_h(\mathbf{u}_I(\tau) - \mathbf{u}_\pi(\tau), \dot{\mathbf{e}}_h(\tau)) \right) d\tau. \end{aligned} \quad (71)$$

Then, we integrate by parts the integral that contains $a(\cdot, \cdot)$ and $a_h(\cdot, \cdot)$, and again use the fact that $\mathbf{e}_h(0) = \dot{\mathbf{e}}_h(0) = 0$, to obtain

$$\begin{aligned} \|\mathbf{e}_h(t)\|^2 &\leq \int_0^t \left(\mathsf{R}_1(\tau) + \left[-m(\ddot{\mathbf{u}}(\tau) - \ddot{\mathbf{u}}_\pi(\tau), \dot{\mathbf{e}}_h(\tau)) + m_h(\ddot{\mathbf{u}}_I(\tau) - \ddot{\mathbf{u}}_\pi(\tau), \dot{\mathbf{e}}_h(\tau)) \right] \right. \\ &\quad \left. + \left[a(\dot{\mathbf{u}}(\tau) - \dot{\mathbf{u}}_\pi(\tau), \mathbf{e}_h(\tau)) - a_h(\dot{\mathbf{u}}_I(\tau) - \dot{\mathbf{u}}_\pi(\tau), \mathbf{e}_h(\tau)) \right] \right) d\tau \\ &\quad + \left[-a(\mathbf{u}(t) - \mathbf{u}_\pi(t), \mathbf{e}_h(t)) + a_h(\mathbf{u}_I(t) - \mathbf{u}_\pi(t), \mathbf{e}_h(t)) \right] \\ &= \int_0^t \left(\mathsf{R}_1(\tau) + \mathsf{R}_2(\tau) + \mathsf{R}_3(\tau) \right) d\tau + \mathsf{R}_4(t), \end{aligned} \quad (72)$$

where terms \mathbf{R}_ℓ , $\ell = 2, 3, 4$, match with the squared parenthesis. For the next development, we do not need an upper bound of term \mathbf{R}_1 . Instead, we have to bound the other three terms in the right-hand side of (72). To bound \mathbf{R}_2 we use the continuity of $m(\cdot, \cdot)$ and $m_h(\cdot, \cdot)$ and the definition of the energy norm $\|\|\cdot\|\|$ given in (58):

$$\begin{aligned} |\mathbf{R}_2| &\leq |m(\ddot{\mathbf{u}} - \ddot{\mathbf{u}}_\pi, \dot{\mathbf{e}}_h)| + |m_h(\ddot{\mathbf{u}}_I - \ddot{\mathbf{u}}_\pi, \dot{\mathbf{e}}_h)| \leq (\|\ddot{\mathbf{u}} - \ddot{\mathbf{u}}_\pi\|_0 + \|\ddot{\mathbf{u}}_I - \ddot{\mathbf{u}}_\pi\|_0) \|\dot{\mathbf{e}}_h\|_0 \\ &\leq (\|\ddot{\mathbf{u}} - \ddot{\mathbf{u}}_\pi\|_0 + \|\ddot{\mathbf{u}}_I - \ddot{\mathbf{u}}_\pi\|_0) \|\|\mathbf{e}_h\|\|. \end{aligned} \quad (73)$$

Similarly, to bound \mathbf{R}_3 we use the continuity of $a(\cdot, \cdot)$ and $a_h(\cdot, \cdot)$ and the definition of the energy norm $\|\|\cdot\|\|$ given in (58):

$$\begin{aligned} |\mathbf{R}_3| &\leq |a(\dot{\mathbf{u}} - \dot{\mathbf{u}}_\pi, \mathbf{e}_h)| + |a_h(\dot{\mathbf{u}}_I - \dot{\mathbf{u}}_\pi, \mathbf{e}_h)| \leq (|\dot{\mathbf{u}} - \dot{\mathbf{u}}_\pi|_{1,h} + |\dot{\mathbf{u}}_I - \dot{\mathbf{u}}_\pi|_1) |\mathbf{e}_h|_1 \\ &\leq (|\dot{\mathbf{u}} - \dot{\mathbf{u}}_\pi|_{1,h} + |\dot{\mathbf{u}}_I - \dot{\mathbf{u}}_\pi|_1) \|\|\mathbf{e}_h\|\|. \end{aligned} \quad (74)$$

Finally, to bound \mathbf{R}_4 we first use the continuity of $a(\cdot, \cdot)$ and $a_h(\cdot, \cdot)$, and the right inequality in (59); then, we apply the Young inequality, so that

$$\begin{aligned} |\mathbf{R}_4| &\leq |a(\mathbf{u} - \mathbf{u}_\pi, \mathbf{e}_h)| + |a_h(\mathbf{u}_I - \mathbf{u}_\pi, \mathbf{e}_h)| \leq (|\mathbf{u} - \mathbf{u}_\pi|_1 + |\mathbf{u}_I - \mathbf{u}_\pi|_1) |\mathbf{e}_h|_1 \\ &\leq (|\mathbf{u} - \mathbf{u}_\pi|_1 + |\mathbf{u}_I - \mathbf{u}_\pi|_1) \|\|\mathbf{e}_h\|\| \leq \frac{1}{2\epsilon} (|\mathbf{u} - \mathbf{u}_\pi|_1 + |\mathbf{u}_I - \mathbf{u}_\pi|_1)^2 + \frac{\epsilon}{2} \|\|\mathbf{e}_h\|\|^2. \end{aligned} \quad (75)$$

Using bounds (73), (74), and (75) in (72), we find the inequality

$$\|\|\mathbf{e}_h(t)\|\|^2 \lesssim \tilde{G}_0^2(t) + \int_0^t G_1(\tau) \|\|\mathbf{e}_h(\tau)\|\| d\tau \lesssim \left(\sup_{\tau \in [0, T]} G_0(\tau) \right)^2 + \int_0^t G_1(\tau) \|\|\mathbf{e}_h(\tau)\|\| d\tau,$$

where $\tilde{G}_0^2(t) = (|\mathbf{u}(\tau) - \mathbf{u}_I(\tau)|_{1,h} + |\mathbf{u}(\tau) - \mathbf{u}_\pi(\tau)|_{1,h})^2$, and $G_0(t)$ and $G_1(t)$ are the time-dependent functions defined in (63)-(64). Again, an application of [47, Lemma A5, p. 157] yields

$$\|\|\mathbf{e}_h(t)\|\| \lesssim \sup_{\tau \in [0, T]} G_0(\tau) + \int_0^t G_1(\tau) d\tau.$$

The theorem follows on using the triangular inequality

$$\|\|\mathbf{u}(t) - \mathbf{u}_h(t)\|\| \leq \|\|\mathbf{u}(t) - \mathbf{u}_I(t)\|\| + \|\|\mathbf{u}_I(t) - \mathbf{u}_h(t)\|\|$$

and noting that $\|\|\mathbf{u}(t) - \mathbf{u}_I(t)\|\|$ is absorbed in $\sup_{\tau \in [0, T]} G_0(\tau)$. \square

Corollary 4.7 *Under the conditions of Theorem 4.6, for $\mathbf{f} \in L^2((0, T); [H^{m-1}(\Omega)]^2)$ we have that*

$$\begin{aligned} \sup_{0 < t \leq T} \|\|\mathbf{u}(t) - \mathbf{u}_h(t)\|\| &\lesssim \frac{h^\mu}{k^m} \sup_{0 < t \leq T} \left(\|\dot{\mathbf{u}}(t)\|_{m+1} + \|\mathbf{u}(t)\|_{m+1} \right) \\ &+ \int_0^T \left(\frac{h^{\mu+1}}{k^m} (\|\ddot{\mathbf{u}}(\tau)\|_{m+1} + \|\dot{\mathbf{u}}(\tau)\|_{m+1}) + \frac{h^\mu}{k^m} (\|\ddot{\mathbf{u}}(\tau)\|_{m+1} + \|\dot{\mathbf{u}}(\tau)\|_{m+1}) \right) d\tau \\ &+ \int_0^T h \|(I - \Pi_{k-2}^0) \mathbf{f}(\tau)\|_0 d\tau, \end{aligned} \quad (76)$$

where $\mu = \min(k, m)$.

Proof. Note that

$$F_h(\mathbf{v}_h) = \int_\Omega \mathbf{f} \cdot \Pi_{k-2}^0 \mathbf{v}_h dV = \int_\Omega \Pi_{k-2}^0 \mathbf{f} \cdot \mathbf{v}_h dV. \quad (77)$$

For all $\mathbf{v}_h \in \mathbf{V}_k^h$ it holds that

$$\begin{aligned} |F(\mathbf{v}_h) - F_h(\mathbf{v}_h)| &= \left| \int_\Omega (I - \Pi_{k-2}^0) \mathbf{f} \cdot \mathbf{v}_h dV \right| = \left| \int_\Omega (I - \Pi_{k-2}^0) \mathbf{f} \cdot (I - \Pi_0^0) \mathbf{v}_h dV \right| \\ &= \|(I - \Pi_{k-2}^0) \mathbf{f}\|_0 \|(I - \Pi_0^0) \mathbf{v}_h\|_0 \lesssim h \|(I - \Pi_{k-2}^0) \mathbf{f}\|_0 |\mathbf{v}_h|_1. \end{aligned} \quad (78)$$

Hence,

$$\sup_{\mathbf{v}_h \in \mathbf{V}_k^h \setminus \{0\}} \frac{|F(\mathbf{v}_h) - F_h(\mathbf{v}_h)|}{|\mathbf{v}_h|_1} \leq h \|(I - \Pi_{k-2}^0)\mathbf{f}\|_0. \quad (79)$$

Estimate (76) follows on applying this inequality and the results of Lemmas 4.1 and 4.2 to (63) and (64), using the resulting estimates in (62), and taking the supremum on the time interval $[0, T]$. \square

4.4. Convergence analysis in the L^2 norm

The main result of this section is the following theorem that proves the L^2 -convergence (with suboptimal rate) of the conforming VEM. The strategy we use in the proof is inspired by Ref. [19], using also the substantial modifications required to set it up in the virtual element framework found in [3].

Theorem 4.8 *Let \mathbf{u} be the exact solution of problem (12) under the assumption that domain Ω is H^2 -regular and $\mathbf{u}_h \in \mathbf{V}_k^h$ the solution of the virtual element method stated in (13) under the mesh assumptions of Section 3.1. If $\mathbf{u}, \dot{\mathbf{u}}, \ddot{\mathbf{u}} \in L^2(0, T; [H^{m+1}(\Omega) \cap H_0^1(\Omega)]^2)$, with integer $m \geq 0$, then the following estimate holds for almost every $t \in [0, T]$ by setting $\mu = \min(m, k)$:*

$$\begin{aligned} \|\mathbf{u}(t) - \mathbf{u}_h(t)\|_0 &\lesssim \|\mathbf{u}_h(0) - \mathbf{u}_0\|_0 + \|\dot{\mathbf{u}}_h(0) - \mathbf{u}_1\|_0 + \frac{h^{\mu+1}}{k^m} \left(\|\ddot{\mathbf{u}}\|_{L^2(0, T; [H^{m+1}(\Omega)]^2)} \right. \\ &\quad \left. + \|\dot{\mathbf{u}}\|_{L^2(0, T; [H^{m+1}(\Omega)]^2)} + \|\mathbf{u}\|_{L^2(0, T; [H^{m+1}(\Omega)]^2)} \right) + \int_0^T \|(1 - \Pi_{k-2}^0)\mathbf{f}(\tau)\|_0^2 d\tau. \end{aligned} \quad (80)$$

The constant hidden by the “ \lesssim ” notation is independent of h , but depends on the regularity constant ϱ of the mesh, the stability constant μ^* , and may not grow faster than $\exp(T^3)$ with respect to the final integration time T .

To prove this theorem, we need the energy projection operator $\mathcal{P}_h : [H_{\Gamma_D}^1(\Omega)]^2 \rightarrow \mathbf{V}_k^h$, which is such that $\mathcal{P}_h \mathbf{u} \in \mathbf{V}_k^h$, for every $\mathbf{u} \in [H_{\Gamma_D}^1(\Omega)]^2$, is the solution of the variational problem:

$$a_h(\mathcal{P}_h \mathbf{u}, \mathbf{v}_h) = a(\mathbf{u}, \mathbf{v}_h) \quad \forall \mathbf{v}_h \in \mathbf{V}_k^h. \quad (81)$$

The energy projection $\mathcal{P}_h \mathbf{u}$ is a virtual element approximation of the exact solution \mathbf{u} , and the accuracy of the approximation is characterized by the following lemma.

Lemma 4.9 *Let $\mathbf{u} \in [H^{m+1}(\Omega) \cap H_0^1(\Omega)]^2$ be the solution of problem (12) under the mesh assumptions of Section 3.1. Then, there exists a unique function $\mathcal{P}_h \mathbf{u} \in \mathbf{V}_k^h$ such that*

$$|\mathbf{u} - \mathcal{P}_h \mathbf{u}|_{1,h} \lesssim \frac{h^\mu}{k^m} \|\mathbf{u}\|_{m+1} \quad (82)$$

with $\mu = \min(k, m)$ and $m \geq 1$. Moreover, if domain Ω is H^2 -regular, it holds that

$$\|\mathbf{u} - \mathcal{P}_h \mathbf{u}\|_0 \lesssim \frac{h^{\mu+1}}{k^m} \|\mathbf{u}\|_{m+1}. \quad (83)$$

Proof. The argument we use in this proof is similar to that used in the proof of [111, Lemma 3.1] for the conforming virtual element approximation of a scalar parabolic problem. Nonetheless, our proof herein differs in several points due to different problem, the vector nature of space \mathbf{V}_k^h and use the hp -interpolation estimates of Lemmas 4.1 and 4.2.

First, we note that the bilinear form $a_h(\cdot, \cdot)$ is continuous and coercive on $\mathbf{V}_k^h \times \mathbf{V}_k^h$, the linear functional $a(\mathbf{u}, \cdot)$ is continuous on \mathbf{V}_k^h , and the Lax-Milgram Lemma implies that the solution $\mathcal{P}_h \mathbf{u}$ to problem (81) exists and is unique. Then, to prove estimate (82), we introduce the virtual element interpolate \mathbf{u}_I of \mathbf{u} , which is the function in \mathbf{V}_k^h that has the same degrees of freedom of \mathbf{u} and satisfies the error inequality given in Lemma 4.2. A straightforward application of the triangular inequality yields:

$$|\mathbf{u} - \mathcal{P}_h \mathbf{u}|_1 \leq |\mathbf{u} - \mathbf{u}_I|_1 + |\mathbf{u}_I - \mathcal{P}_h \mathbf{u}|_1, \quad (84)$$

We estimate the first term on the right by using the first inequality in (57). Instead, to estimate the second term we need the following developments. Let $\delta_h = \mathcal{P}_h \mathbf{u} - \mathbf{u}_I$ and \mathbf{u}_π any piecewise polynomial approximation of degree (at most) k that satisfies inequality (56) on each element P . Using the k -consistency property, stability, and the continuity of the bilinear forms a_h and a yield the development chain:

$$\begin{aligned}
\alpha_* |\delta_h|_{1,h}^2 &= \alpha_* a(\delta_h, \delta_h) \leq a_h(\delta_h, \delta_h) = a_h(\mathcal{P}_h \mathbf{u}, \delta_h) - a_h(\mathbf{u}_I, \delta_h) = a(\mathbf{u}, \delta_h) - a_h(\mathbf{u}_I, \delta_h) \\
&= \sum_{\mathsf{P} \in \Omega_h} \left(a^{\mathsf{P}}(\mathbf{u}, \delta_h) - a_h^{\mathsf{P}}(\mathbf{u}_I, \delta_h) \right) \\
&= \sum_{\mathsf{P} \in \Omega_h} \left(a^{\mathsf{P}}(\mathbf{u} - \mathbf{u}_\pi, \delta_h) - a_h^{\mathsf{P}}(\mathbf{u}_I - \mathbf{u}_\pi, \delta_h) \right) \\
&\leq \sum_{\mathsf{P} \in \Omega_h} \left(|\mathbf{u} - \mathbf{u}_\pi|_{1,\mathsf{P}} + \alpha^* |\mathbf{u}_I - \mathbf{u}_\pi|_{1,\mathsf{P}} \right) |\delta_h|_{1,\mathsf{P}} \\
&\lesssim \max(1, \alpha^*) \left(|\mathbf{u} - \mathbf{u}_\pi|_{1,h} + |\mathbf{u}_I - \mathbf{u}_\pi|_{1,h} \right) |\delta_h|_{1,h}.
\end{aligned}$$

Therefore, it holds that

$$|\mathcal{P}_h \mathbf{u} - \mathbf{u}_I|_{1,h} \lesssim \left(|\mathbf{u} - \mathbf{u}_\pi|_{1,h} + |\mathbf{u}_I - \mathbf{u}_\pi|_{1,h} \right) \lesssim \left(2|\mathbf{u} - \mathbf{u}_\pi|_{1,h} + |\mathbf{u}_I - \mathbf{u}|_1 \right).$$

Inequality (82) follows on substituting this relation in (84) and using (56).

To derive the estimate in the L^2 -norm, we consider the weak solution $\psi \in [H^2(\Omega)]^2 \cap [H_{\Gamma_D}^1(\Omega)]^2$ to the auxiliary elliptic equation:

$$\begin{aligned}
-\nabla \cdot \boldsymbol{\sigma}(\psi) &= \mathbf{u} - \mathcal{P}_h \mathbf{u} && \text{in } \Omega, \\
\psi &= \mathbf{0} && \text{on } \Gamma,
\end{aligned}$$

which satisfies, as Ω is an H^2 -regular domain, the following stability result:

$$\|\psi\|_2 \leq \mathcal{C} \|\mathbf{u} - \mathcal{P}_h \mathbf{u}\|_0. \quad (85)$$

Let $\psi^I \in \mathbf{V}_k^h$ be the virtual element interpolate of ψ that satisfies the interpolation error estimate given in Lemma 4.2 (with $m = 1$). We integrate by parts and use the definition of the energy projection \mathcal{P}_h :

$$\begin{aligned}
\|\mathbf{u} - \mathcal{P}_h \mathbf{u}\|_0^2 &= (\mathbf{u} - \mathcal{P}_h \mathbf{u}, \mathbf{u} - \mathcal{P}_h \mathbf{u}) = (\mathbf{u} - \mathcal{P}_h \mathbf{u}, -\nabla \cdot \boldsymbol{\sigma}(\psi)) = a(\mathbf{u} - \mathcal{P}_h \mathbf{u}, \psi) \\
&= a(\mathbf{u} - \mathcal{P}_h \mathbf{u}, \psi - \psi^I) + a(\mathbf{u} - \mathcal{P}_h \mathbf{u}, \psi^I) \\
&= \mathsf{T}_1 + \mathsf{T}_2.
\end{aligned} \quad (86)$$

The proof continues by estimating each term T_i , $i = 1, 2$, separately. The first term is bounded as follows:

$$\begin{aligned}
|\mathsf{T}_1| &= |a(\mathbf{u} - \mathcal{P}_h \mathbf{u}, \psi - \psi^I)| \leq \|\mathbf{u} - \mathcal{P}_h \mathbf{u}\|_{1,h} \|\psi - \psi^I\|_{1,h} \lesssim \frac{h^\mu}{k^m} \|\mathbf{u}\|_{m+1} h |\psi|_2 \\
&\lesssim \frac{h^{\mu+1}}{k^m} \|\mathbf{u}\|_{m+1} \|\mathbf{u} - \mathcal{P}_h \mathbf{u}\|_0
\end{aligned}$$

where we used the estimate in the energy norm (82) derived previously and interpolation error estimate (57). For the second term, first we use the consistency and stability property to transform T_2 as follows:

$$\begin{aligned}
\mathsf{T}_2 &= a(\mathbf{u}, \psi^I) - a(\mathcal{P}_h \mathbf{u}, \psi^I) = \sum_{\mathsf{P} \in \Omega_h} \left(a_h^{\mathsf{P}}(\mathcal{P}_h \mathbf{u}, \psi^I) - a^{\mathsf{P}}(\mathcal{P}_h \mathbf{u}, \psi^I) \right) \\
&= \sum_{\mathsf{P} \in \Omega_h} \left(a_h^{\mathsf{P}}(\mathcal{P}_h \mathbf{u} - \mathbf{u}_\pi, \psi^I - \Pi_1^0 \psi) - a^{\mathsf{P}}(\mathcal{P}_h \mathbf{u} - \mathbf{u}_\pi, \psi^I - \Pi_1^0 \psi) \right).
\end{aligned}$$

Then, we add and subtract \mathbf{u} and ψ and use estimates (56) and (57) to obtain

$$\begin{aligned}
|\mathbf{T}_2| &\leq \max(1, \alpha^*) \sum_{\mathbf{P} \in \Omega_h} |\mathcal{P}_h \mathbf{u} - \mathbf{u}_\pi|_{1,\mathbf{P}} |\psi^I - \Pi_1^0 \psi|_{1,\mathbf{P}} \\
&\leq \max(1, \alpha^*) \sum_{\mathbf{P} \in \Omega_h} (|\mathcal{P}_h \mathbf{u} - \mathbf{u}|_{1,\mathbf{P}} + |\mathbf{u} - \mathbf{u}_\pi|_{1,\mathbf{P}}) (|\psi^I - \psi|_{1,\mathbf{P}} + |\psi - \Pi_1^0 \psi|_{1,\mathbf{P}}) \\
&\lesssim \sum_{\mathbf{P} \in \Omega_h} \frac{h_\mathbf{P}^\mu}{k^m} |\mathbf{u}|_{m+1,\mathbf{P}} h_\mathbf{P} |\psi|_{2,\mathbf{P}} \lesssim \frac{h^{\mu+1}}{k^m} |\mathbf{u}|_{m+1} \|\psi\|_2 \\
&\lesssim \frac{h^{\mu+1}}{k^m} |\mathbf{u}|_{m+1} \|\mathbf{u} - \mathcal{P}_h \mathbf{u}\|_0,
\end{aligned}$$

and the bound of \mathbf{T}_2 is derived by using in the final step the H^2 -regularity of ψ . The estimate in the L^2 -norm is finally proved by collecting the estimates of the two terms \mathbf{T}_i , $i = 1, 2$. \square

Proof of Theorem 4.8. We use the energy projection to split the approximation error as follows: $\mathbf{u}(t) - \mathbf{u}_h(t) = \rho(t) - \eta(t)$, with $\rho(t) = \mathbf{u}(t) - \mathcal{P}_h \mathbf{u}(t)$ and $\eta(t) = \mathbf{u}_h(t) - \mathcal{P}_h \mathbf{u}(t)$. Since \mathbf{V}_k^h is a subspace of $[H_{\Gamma_D}^1(\Omega)]^2$, to derive the error equation, we test (12) and (13) against $\mathbf{v}_h \in \mathbf{V}_k^h$

$$\begin{aligned}
m(\ddot{\mathbf{u}}, \mathbf{v}_h) + a(\mathbf{u}, \mathbf{v}_h) &= F(\mathbf{v}_h), \\
m_h(\ddot{\mathbf{u}}_h, \mathbf{v}_h) + a_h(\mathbf{u}_h, \mathbf{v}_h) &= F_h(\mathbf{v}_h),
\end{aligned}$$

and take the difference

$$m_h(\ddot{\mathbf{u}}_h, \mathbf{v}_h) + a_h(\mathbf{u}_h, \mathbf{v}_h) - (m(\ddot{\mathbf{u}}, \mathbf{v}_h) + a(\mathbf{u}, \mathbf{v}_h)) = F_h(\mathbf{v}_h) - F(\mathbf{v}_h). \quad (87)$$

We add and subtract $\mathcal{P}_h \ddot{\mathbf{u}}$ and $\mathcal{P}_h \mathbf{u}$ in the virtual element bilinear forms m_h and a_h and rearrange the terms containing $\ddot{\mathbf{u}}$ and \mathbf{u} to the right-hand side to obtain:

$$\begin{aligned}
m_h(\ddot{\mathbf{u}}_h - \mathcal{P}_h \ddot{\mathbf{u}}, \mathbf{v}_h) + a_h(\mathbf{u}_h - \mathcal{P}_h \mathbf{u}, \mathbf{v}_h) &= F_h(\mathbf{v}_h) - F(\mathbf{v}_h) + m(\ddot{\mathbf{u}}, \mathbf{v}_h) + a(\mathbf{u}, \mathbf{v}_h) \\
&\quad - m_h(\mathcal{P}_h \ddot{\mathbf{u}}, \mathbf{v}_h) - a_h(\mathcal{P}_h \mathbf{u}, \mathbf{v}_h).
\end{aligned} \quad (88)$$

Since (81) implies that $a(\mathbf{u}, \mathbf{v}_h) - a_h(\mathcal{P}_h \mathbf{u}, \mathbf{v}_h) = 0$, and using the notation $\ddot{\boldsymbol{\eta}} = \ddot{\mathbf{u}}_h - \mathcal{P}_h \ddot{\mathbf{u}}$ and $\boldsymbol{\eta} = \mathbf{u}_h - \mathcal{P}_h \mathbf{u}$, we obtain

$$m_h(\ddot{\boldsymbol{\eta}}, \mathbf{v}_h) + a_h(\boldsymbol{\eta}, \mathbf{v}_h) = F_h(\mathbf{v}_h) - F(\mathbf{v}_h) + m(\ddot{\mathbf{u}}, \mathbf{v}_h) - m_h(\mathcal{P}_h \ddot{\mathbf{u}}, \mathbf{v}_h). \quad (89)$$

Hereafter in this proof, we will assume that

$$\mathbf{v}_h(t) = \int_t^\xi \boldsymbol{\eta}(\tau) d\tau \quad (90)$$

for every t and $\xi \in [0, T]$. The function $\mathbf{v}_h(t)$ given by (90) obviously belongs to the virtual element space \mathbf{V}_k^h as it is a linear superposition of virtual element functions in such a space and, thus, can be used as a test function. Since now \mathbf{v}_h depends on time t , we are allowed to consider its time derivatives. In particular, we observe that the straightforward calculation

$$\frac{d}{dt} \left(\mathbf{v}_h \frac{d}{dt} (\mathbf{u} - \mathbf{u}_h) \right) = \frac{d}{dt} \left(\mathbf{v}_h \frac{d}{dt} (\boldsymbol{\rho} - \boldsymbol{\eta}) \right) = \frac{d\mathbf{v}_h}{dt} \frac{d\boldsymbol{\rho}}{dt} - \frac{d\mathbf{v}_h}{dt} \frac{d\boldsymbol{\eta}}{dt} + \mathbf{v}_h \frac{d^2 \boldsymbol{\rho}}{dt^2} - \mathbf{v}_h \frac{d^2 \boldsymbol{\eta}}{dt^2}$$

implies the identity

$$m_h(\ddot{\boldsymbol{\eta}}, \mathbf{v}_h) = -m_h(\dot{\boldsymbol{\eta}}, \dot{\mathbf{v}}_h) - \frac{d}{dt} m_h(\dot{\mathbf{u}} - \dot{\mathbf{u}}_h, \mathbf{v}_h) + m_h(\ddot{\boldsymbol{\rho}}, \mathbf{v}_h) + m_h(\dot{\boldsymbol{\rho}}, \dot{\mathbf{v}}_h). \quad (91)$$

Therefore, using (91) in (89) yields

$$\begin{aligned}
-m_h(\dot{\boldsymbol{\eta}}, \dot{\mathbf{v}}_h) + a_h(\boldsymbol{\eta}, \mathbf{v}_h) &= F_h(\mathbf{v}_h) - F(\mathbf{v}_h) + m(\ddot{\mathbf{u}}, \mathbf{v}_h) - m_h(\mathcal{P}_h \ddot{\mathbf{u}}, \mathbf{v}_h) \\
&\quad + \frac{d}{dt} m_h(\dot{\mathbf{u}} - \dot{\mathbf{u}}_h, \mathbf{v}_h) - m_h(\ddot{\boldsymbol{\rho}}, \mathbf{v}_h) - m_h(\dot{\boldsymbol{\rho}}, \dot{\mathbf{v}}_h).
\end{aligned} \quad (92)$$

We rewrite the approximation error on the source term on the right-hand side of (92) as follows:

$$F_h(\mathbf{v}_h(t)) - F(\mathbf{v}_h(t)) = m(\mathbf{f}_h(t) - \mathbf{f}(t), \mathbf{v}_h(t)), \quad (93)$$

where $\mathbf{f}_h(t) = \Pi_{k-2}^0 \mathbf{f}$ according to (34). Following [3], we consider the integral quantities

$$\mathcal{A}_1(t) = \int_0^t (\mathbf{f}_h(\tau) - \mathbf{f}(\tau)) d\tau, \quad \mathcal{A}_2(t) = \int_0^t \ddot{\mathbf{u}}(\tau) d\tau, \quad \mathcal{A}_3(t) = \int_0^t \mathcal{P}_h \ddot{\mathbf{u}}(\tau) d\tau, \quad (94)$$

and note that

$$F_h(\mathbf{v}_h(t)) - F(\mathbf{v}_h(t)) = \frac{d}{dt} m(\mathcal{A}_1, \mathbf{v}_h) - m(\mathcal{A}_1, \dot{\mathbf{v}}_h), \quad (95)$$

$$m(\ddot{\mathbf{u}}, \mathbf{v}_h) = \frac{d}{dt} m(\mathcal{A}_2, \mathbf{v}_h) - m(\mathcal{A}_2, \dot{\mathbf{v}}_h), \quad (96)$$

$$m_h(\mathcal{P}_h \ddot{\mathbf{u}}, \mathbf{v}_h) = \frac{d}{dt} m_h(\mathcal{A}_3, \mathbf{v}_h) - m_h(\mathcal{A}_3, \dot{\mathbf{v}}_h). \quad (97)$$

Hence, using (95), (96) and (97) in (92) yields

$$\begin{aligned} -m_h(\dot{\boldsymbol{\eta}}, \dot{\mathbf{v}}_h) + a_h(\boldsymbol{\eta}, \mathbf{v}_h) &= \sum_{i=1}^2 \left[\frac{d}{dt} m(\mathcal{A}_i, \mathbf{v}_h) - m(\mathcal{A}_i, \dot{\mathbf{v}}_h) \right] - \left[\frac{d}{dt} m_h(\mathcal{A}_3, \mathbf{v}_h) - m_h(\mathcal{A}_3, \dot{\mathbf{v}}_h) \right] \\ &\quad + \frac{d}{dt} m_h(\dot{\mathbf{u}} - \dot{\mathbf{u}}_h, \mathbf{v}_h) - m_h(\ddot{\boldsymbol{\rho}}, \mathbf{v}_h) - m_h(\dot{\boldsymbol{\rho}}, \dot{\mathbf{v}}_h). \end{aligned} \quad (98)$$

To prove the assertion of the theorem we integrate both sides of (98) with respect to t between 0 and ξ ; then, we estimate a lower bound for the left-hand side and an upper bound for the right-hand side.

To estimate a lower bound for the left-hand side of (98), we note that $\dot{\mathbf{v}}_h = -\boldsymbol{\eta}$, $\mathbf{v}_h(\xi) = 0$ and $a_h(\mathbf{v}_h(0), \mathbf{v}_h(0)) \geq 0$ from the coercivity of a_h . Thus, we estimate the left-hand side as follows:

$$\begin{aligned} \int_0^\xi [\text{LHS of Eq. (98)}] dt &= \int_0^\xi [m_h(\dot{\boldsymbol{\eta}}, \boldsymbol{\eta}) - a_h(\dot{\mathbf{v}}_h, \mathbf{v}_h)] dt \\ &= \int_0^\xi \frac{1}{2} \frac{d}{dt} [m_h(\boldsymbol{\eta}, \boldsymbol{\eta}) - a_h(\mathbf{v}_h, \mathbf{v}_h)] dt \\ &= \frac{1}{2} [m_h(\boldsymbol{\eta}(\xi), \boldsymbol{\eta}(\xi)) - m_h(\boldsymbol{\eta}(0), \boldsymbol{\eta}(0))] - \frac{1}{2} [a_h(\mathbf{v}_h(\xi), \mathbf{v}_h(\xi)) - a_h(\mathbf{v}_h(0), \mathbf{v}_h(0))] \\ &\geq \frac{1}{2} (m_h(\boldsymbol{\eta}(\xi), \boldsymbol{\eta}(\xi)) - m_h(\boldsymbol{\eta}(0), \boldsymbol{\eta}(0))). \end{aligned} \quad (99)$$

To estimate an upper bound for the right-hand side of (98), we note that $\mathcal{A}_i(0) = 0$ for $i = 1, 2, 3$ and use again the fact $\mathbf{v}_h(\xi) = 0$. So, for $i = 1, 2$, a direct integration yield

$$\begin{aligned} \int_0^\xi \left[\frac{d}{dt} m(\mathcal{A}_i, \mathbf{v}_h) - m(\mathcal{A}_i, \dot{\mathbf{v}}_h) \right] dt &= m(\mathcal{A}_i(\xi), \mathbf{v}_h(\xi)) - m(\mathcal{A}_i(0), \mathbf{v}_h(0)) - \int_0^\xi m(\mathcal{A}_i, \dot{\mathbf{v}}_h) dt \\ &= - \int_0^\xi m(\mathcal{A}_i, \dot{\mathbf{v}}_h) dt \end{aligned} \quad (100)$$

and, similarly,

$$\begin{aligned} \int_0^\xi \left[\frac{d}{dt} m_h(\mathcal{A}_3, \mathbf{v}_h) - m_h(\mathcal{A}_3, \dot{\mathbf{v}}_h) \right] dt &= m_h(\mathcal{A}_3(\xi), \mathbf{v}_h(\xi)) - m_h(\mathcal{A}_3(0), \mathbf{v}_h(0)) - \int_0^\xi m_h(\mathcal{A}_3, \dot{\mathbf{v}}_h) dt \\ &= - \int_0^\xi m_h(\mathcal{A}_3, \dot{\mathbf{v}}_h) dt. \end{aligned} \quad (101)$$

Using (100) and (101) in the right-hand side of (98) and rearranging the terms yield

$$\begin{aligned} \int_0^\xi [\text{RHS of Eq. (98)}] dt &= - \int_0^\xi m(\mathcal{A}_1, \dot{\mathbf{v}}_h) dt + \int_0^\xi (m_h(\mathcal{A}_3, \dot{\mathbf{v}}_h) - m(\mathcal{A}_2, \dot{\mathbf{v}}_h)) dt \\ &\quad + \left[m_h(\dot{\mathbf{u}}(\xi) - \dot{\mathbf{u}}_h(\xi), \mathbf{v}_h(\xi)) - m_h(\dot{\mathbf{u}}(0) - \dot{\mathbf{u}}_h(0), \mathbf{v}_h(0)) \right] \\ &\quad - \int_0^\xi (m_h(\ddot{\rho}, \mathbf{v}_h) + m_h(\dot{\rho}, \dot{\mathbf{v}}_h)) dt = \mathsf{L}_1(\xi) + \mathsf{L}_2(\xi) + \mathsf{L}_3(\xi) + \mathsf{L}_4(\xi). \end{aligned}$$

The proof continues by bounding the four terms $\mathsf{L}_i(\xi)$, $i = 1, 2, 3, 4$, separately.

Estimate of term L_1 . To estimate L_1 , we first note that $m(\cdot, \cdot)$ is an inner product, so we can apply the Cauchy-Schwarz and the Young inequalities to derive the following bound, which holds for any $t \in [0, \xi]$:

$$|m(\mathcal{A}_1(t), \dot{\mathbf{v}}_h(t))| \leq \|\mathcal{A}_1(t)\|_0 \|\dot{\mathbf{v}}_h(t)\|_0 \leq \frac{1}{2} \|\mathcal{A}_1(t)\|_0^2 + \frac{1}{2} \|\dot{\mathbf{v}}_h(t)\|_0^2. \quad (102)$$

We estimate term $\|\mathcal{A}_1(t)\|_0$ by applying Jensen's inequality and Fubini's theorem to exchange the integration order

$$\begin{aligned} \|\mathcal{A}_1(t)\|_0^2 &= \int_{\Omega} \left| \int_0^t (\mathbf{f}(\tau) - \Pi_{k-2}^0(\mathbf{f}(\tau)) d\tau \right|^2 dV \leq \int_{\Omega} T \left(\int_0^t |(I - \Pi_{k-2}^0)\mathbf{f}(\tau)|^2 d\tau \right) dV \\ &= T \int_0^t \left(\int_{\Omega} |(I - \Pi_{k-2}^0)\mathbf{f}(\tau)|^2 dV \right) d\tau \leq T \int_0^t \|(I - \Pi_{k-2}^0)\mathbf{f}(\tau)\|_0^2 d\tau. \\ &\leq T \int_0^T \|(I - \Pi_{k-2}^0)\mathbf{f}(\tau)\|_0^2 d\tau. \end{aligned} \quad (103)$$

We use (103) in (102) and the resulting inequality in the definition of L_1 ; then, we note that the last integral in (103) is on the whole interval $[0, T]$, and is, thus, independent on t . Since $\xi \leq T$ and by using the Young's inequality, we readily find that

$$\begin{aligned} |\mathsf{L}_1(\xi)| &\leq \left| \int_0^\xi (m(\mathcal{A}_1(t), \dot{\mathbf{v}}_h(t))) dt \right| \leq \int_0^\xi |m(\mathcal{A}_1(t), \dot{\mathbf{v}}_h(t))| dt \leq \frac{1}{2} \int_0^\xi \|\mathcal{A}_1(t)\|_0^2 dt + \frac{1}{2} \int_0^\xi \|\dot{\mathbf{v}}_h(t)\|_0^2 dt \\ &\leq \frac{T^2}{2} \int_0^T \|(I - \Pi_{k-2}^0)\mathbf{f}(\tau)\|_0^2 d\tau + \frac{1}{2} \int_0^\xi \|\dot{\mathbf{v}}_h(t)\|_0^2 dt. \end{aligned}$$

Estimate of term L_2 . Let $\ddot{\mathbf{u}}_\pi$ be any piecewise polynomial approximation of degree at most k of $\ddot{\mathbf{u}}$ that satisfies Lemma 4.1. Now, consider the piecewise polynomial function defined on mesh Ω_h that is given by

$$(\mathcal{A}_2)_\pi = \int_0^t \ddot{\mathbf{u}}_\pi(\tau) d\tau.$$

Then, we start the estimate of the integral argument of L_2 by using consistency property (26) to add and subtract $(\mathcal{A}_2)_\pi$:

$$\begin{aligned}
|m(\mathcal{A}_2, \dot{\mathbf{v}}_h) - m_h(\mathcal{A}_3, \dot{\mathbf{v}}_h)| &= |m(\mathcal{A}_2 - (\mathcal{A}_2)_\pi, \dot{\mathbf{v}}_h) - m_h(\mathcal{A}_3 - (\mathcal{A}_2)_\pi, \dot{\mathbf{v}}_h)| && [\text{add and subtract } \mathcal{A}_2] \\
&= |m(\mathcal{A}_2 - (\mathcal{A}_2)_\pi, \dot{\mathbf{v}}_h) - m_h(\mathcal{A}_3 - \mathcal{A}_2, \dot{\mathbf{v}}_h) - m_h(\mathcal{A}_2 - (\mathcal{A}_2)_\pi, \dot{\mathbf{v}}_h)| && [\text{use triangular inequality}] \\
&\leq |m(\mathcal{A}_2 - (\mathcal{A}_2)_\pi, \dot{\mathbf{v}}_h)| + |m_h(\mathcal{A}_3 - \mathcal{A}_2, \dot{\mathbf{v}}_h)| + |m_h(\mathcal{A}_2 - (\mathcal{A}_2)_\pi, \dot{\mathbf{v}}_h)| && [\text{use (32) and continuity of } m] \\
&\leq \left((1 + \mu^*) \|\mathcal{A}_2 - (\mathcal{A}_2)_\pi\|_0 + \mu^* \|\mathcal{A}_3 - \mathcal{A}_2\|_0 \right) \|\dot{\mathbf{v}}_h\|_0 && [\text{note that } \mu^* < 1 + \mu^*] \\
&\leq (1 + \mu^*) \left(\|\mathcal{A}_2 - (\mathcal{A}_2)_\pi\|_0 + \|\mathcal{A}_3 - \mathcal{A}_2\|_0 \right) \|\dot{\mathbf{v}}_h\|_0 && [\text{use Young's inequality}] \\
&\leq \frac{(1 + \mu^*)}{2} \left(\|\mathcal{A}_2 - (\mathcal{A}_2)_\pi\|_0 + \|\mathcal{A}_3 - \mathcal{A}_2\|_0 \right)^2 + \frac{(1 + \mu^*)}{2} \|\dot{\mathbf{v}}_h\|_0^2 && [\text{use } (a + b)^2 \leq 2a^2 + 2b^2] \\
&\leq (1 + \mu^*) \left(\|\mathcal{A}_2 - (\mathcal{A}_2)_\pi\|_0^2 + \|\mathcal{A}_3 - \mathcal{A}_2\|_0^2 \right) + \frac{(1 + \mu^*)}{2} \|\dot{\mathbf{v}}_h\|_0^2.
\end{aligned}$$

To estimate $\|\mathcal{A}_2(t) - (\mathcal{A}_2(t))_\pi\|_0^2$, we start from the definition of $\mathcal{A}_2(t)$ and $(\mathcal{A}_2(t))_\pi$:

$$\begin{aligned}
\|\mathcal{A}_2(t) - (\mathcal{A}_2(t))_\pi\|_0^2 &= \left\| \int_0^t (\ddot{\mathbf{u}}(\tau) - \ddot{\mathbf{u}}_\pi(\tau)) d\tau \right\|_0^2 && [\text{use definition of } L^2(\Omega)\text{-norm}] \\
&= \int_{\Omega} \left| \int_0^t (\ddot{\mathbf{u}}(\tau) - \ddot{\mathbf{u}}_\pi(\tau)) d\tau \right|^2 dV && [\text{use Jensen's inequality}] \\
&\leq \int_{\Omega} \left(\int_0^t |\ddot{\mathbf{u}}(\tau) - \ddot{\mathbf{u}}_\pi(\tau)|^2 d\tau \right) dV && [\text{apply Fubini's Theorem}] \\
&\leq T \int_0^t \left(\int_{\Omega} |\ddot{\mathbf{u}}(\tau) - \ddot{\mathbf{u}}_\pi(\tau)|^2 dV \right) d\tau && [\text{use definition of } L^2(\Omega)\text{-norm}] \\
&= T \int_0^t \|\ddot{\mathbf{u}}(\tau) - \ddot{\mathbf{u}}_\pi(\tau)\|_0^2 d\tau && [\text{apply Lemma 4.1}] \\
&\lesssim T \frac{h^{2(\mu+1)}}{k^{2(m+1)}} \int_0^t \|\ddot{\mathbf{u}}(\tau)\|_{m+1}^2 d\tau && [\text{use definition of } L^2(0, T; [H^{m+1}(\Omega)]^2)\text{-norm}] \\
&\lesssim T \frac{h^{2(\mu+1)}}{k^{2(m+1)}} \|\ddot{\mathbf{u}}\|_{L^2(0, T; [H^{m+1}(\Omega)]^2)}^2.
\end{aligned}$$

Similarly, to estimate $\|\mathcal{A}_3(t) - \mathcal{A}_2(t)\|_0^2$, we start from the definition of $\mathcal{A}_3(t)$ and $\mathcal{A}_2(t)$:

$$\begin{aligned}
\|\mathcal{A}_3(t) - \mathcal{A}_2(t)\|_0^2 &= \left\| \int_0^t \left(\mathcal{P}_h \ddot{\mathbf{u}}(\tau) - \ddot{\mathbf{u}}(\tau) \right) d\tau \right\|_0^2 && [\text{use definition of } L^2(\Omega)\text{-norm}] \\
&= \int_{\Omega} \left| \int_0^t \left(\mathcal{P}_h \ddot{\mathbf{u}}(\tau) - \ddot{\mathbf{u}}(\tau) \right) d\tau \right|^2 dV && [\text{use Jensen's inequality}] \\
&\leq \int_{\Omega} \left(\int_0^t |\mathcal{P}_h \ddot{\mathbf{u}}(\tau) - \ddot{\mathbf{u}}(\tau)|^2 d\tau \right) dV && [\text{apply Fubini's Theorem}] \\
&\leq T \int_0^t \left(\int_{\Omega} |\mathcal{P}_h \ddot{\mathbf{u}}(\tau) - \ddot{\mathbf{u}}(\tau)|^2 dV \right) d\tau && [\text{use definition of } L^2(\Omega)\text{-norm}] \\
&= T \int_0^t \|\mathcal{P}_h \ddot{\mathbf{u}}(\tau) - \ddot{\mathbf{u}}(\tau)\|_0^2 d\tau && [\text{apply Lemma 4.9 }] \\
&\lesssim T \frac{h^{2(\mu+1)}}{k^{2m}} \int_0^t \|\ddot{\mathbf{u}}(\tau)\|_{m+1}^2 d\tau && [\text{use definition of } L^2(0, T; [H^{m+1}(\Omega)]^2)\text{-norm}] \\
&\lesssim T \frac{h^{2(\mu+1)}}{k^{2m}} \|\ddot{\mathbf{u}}\|_{L^2(0, T; [H^{m+1}(\Omega)]^2)}^2.
\end{aligned}$$

Using the previous estimates, and noting that the integration on the time interval $[0, \xi]$, $\xi \leq T$, produces an additional factor T , we obtain the final upper bound for term L_2 :

$$|\mathsf{L}_2(\xi)| \leq \int_0^{\xi} |m_h(\mathcal{A}_3, \dot{\mathbf{v}}_h) - m(\mathcal{A}_2, \dot{\mathbf{v}}_h)| dt \lesssim T^2 \frac{h^{2(\mu+1)}}{k^{2m}} \|\ddot{\mathbf{u}}\|_{L^2(0, T; [H^{m+1}(\Omega)]^2)}^2 + \frac{1+\mu^*}{2} \int_0^{\xi} \|\dot{\mathbf{v}}_h\|_0^2 dt.$$

Estimate of term L_3 . Since $\mathbf{v}_h(\xi) = 0$ by definition, term L_3 only depends on the approximation error on $\dot{\mathbf{u}}(0) = \mathbf{u}_1$, i.e., the initial condition for $\dot{\mathbf{u}}$. Using (32) and Young's inequality yield:

$$\begin{aligned}
|\mathsf{L}_3(\xi)| &= |m_h(\dot{\mathbf{u}}(0) - \dot{\mathbf{u}}_h(0), \mathbf{v}_h(0))| \leq \mu^* \|\dot{\mathbf{u}}(0) - \dot{\mathbf{u}}_h(0)\|_0 \|\mathbf{v}_h(0)\|_0 \\
&\leq \frac{(\mu^*)^2}{2} \|\dot{\mathbf{u}}(0) - \dot{\mathbf{u}}_h(0)\|_0^2 + \frac{(\mu^*)^2}{2} \|\mathbf{v}_h(0)\|_0^2.
\end{aligned}$$

Estimate of term L_4 . We start from the definition of term L_4 and apply the triangular inequality to find that:

$$|\mathsf{L}_4(\xi)| = \left| \int_0^{\xi} \left(m_h(\ddot{\rho}, \mathbf{v}_h) + m_h(\dot{\rho}, \dot{\mathbf{v}}_h) \right) dt \right| \leq \int_0^{\xi} |m_h(\ddot{\rho}, \mathbf{v}_h)| dt + \int_0^{\xi} |m_h(\dot{\rho}, \dot{\mathbf{v}}_h)| dt. \quad (104)$$

Both terms on the right depend on the exact solution \mathbf{u} and its approximation provided by the energy projection $\mathcal{P}_h \mathbf{u}$. We bound the first term by starting from (32):

$$\begin{aligned}
\int_0^{\xi} |m_h(\ddot{\rho}, \mathbf{v}_h)| dt &\leq \mu^* \int_0^{\xi} \|\ddot{\rho}\|_0 \|\mathbf{v}_h\|_0 dt && [\text{use Young's inequality}] \\
&\leq \frac{\mu^*}{2} \int_0^{\xi} \|\ddot{\rho}\|_0^2 dt + \frac{\mu^*}{2} \int_0^{\xi} \|\mathbf{v}_h\|_0^2 dt && [\text{apply Lemma 4.9 to } \ddot{\rho}] \\
&\lesssim \frac{\mu^* h^{2(\mu+1)}}{2 k^{2m}} \int_0^{\xi} \|\ddot{\mathbf{u}}\|_{m+1}^2 dt + \frac{\mu^*}{2} \int_0^{\xi} \|\mathbf{v}_h\|_0^2 dt && [\text{use definition of } L^2(0, T; [H^{m+1}(\Omega)]^2)\text{-norm}] \\
&\lesssim \frac{\mu^* h^{2(\mu+1)}}{2 k^{2m}} \|\ddot{\mathbf{u}}\|_{L^2(0, T; [H^{m+1}(\Omega)]^2)}^2 + \frac{\mu^*}{2} \int_0^{\xi} \|\mathbf{v}_h\|_0^2 dt.
\end{aligned}$$

Similarly, we bound the second term by starting from (32):

$$\begin{aligned}
\int_0^\xi |m_h(\dot{\rho}, \dot{\mathbf{v}}_h)| dt &\leq \mu^* \int_0^\xi \|\dot{\rho}\|_0 \|\dot{\mathbf{v}}_h\|_0 dt && \text{[use Young's inequality]} \\
&\leq \frac{\mu^*}{2} \int_0^\xi \|\dot{\rho}\|_0^2 dt + \frac{\mu^*}{2} \int_0^\xi \|\dot{\mathbf{v}}_h\|_0^2 dt && \text{[apply Lemma (4.9) to } \dot{\rho} \text{]} \\
&\lesssim \frac{\mu^* h^{2(\mu+1)}}{2 k^{2m}} \int_0^\xi |\dot{\mathbf{u}}|_{m+1}^2 dt + \frac{\mu^*}{2} \int_0^\xi \|\dot{\mathbf{v}}_h\|_0^2 dt && \text{[use definition of } L^2(0, T; [H^{m+1}(\Omega)]^2) \text{-norm]} \\
&\lesssim \frac{\mu^* h^{2(\mu+1)}}{2 k^{2m}} \|\dot{\mathbf{u}}\|_{L^2(0, T; [H^{m+1}(\Omega)]^2)}^2 + \frac{\mu^*}{2} \int_0^\xi \|\dot{\mathbf{v}}_h\|_0^2 dt.
\end{aligned}$$

Using these two estimates in (104), we immediately find that

$$|\mathsf{L}_4(\xi)| \lesssim \frac{\mu^* h^{2(\mu+1)}}{2 k^{2m}} \left(\|\ddot{\mathbf{u}}\|_{L^2(0, T; [H^{m+1}(\Omega)]^2)}^2 + \|\dot{\mathbf{u}}\|_{L^2(0, T; [H^{m+1}(\Omega)]^2)}^2 \right) + \mu^* \int_0^\xi \|\dot{\mathbf{v}}_h\|_0^2 dt. \quad (105)$$

Estimate of $\|\boldsymbol{\eta}\|_0$ and conclusion of the proof. On collecting the upper bounds of $\mathsf{L}_i(\xi)$, $i = 1, 2, 3, 4$, and using the lower bound (99), we have that

$$\begin{aligned}
\mu_* \|\boldsymbol{\eta}(\xi)\|_0^2 &= \mu_* m(\boldsymbol{\eta}(\xi), \boldsymbol{\eta}(\xi)) \leq m_h(\boldsymbol{\eta}(\xi), \boldsymbol{\eta}(\xi)) \\
&\lesssim m_h(\boldsymbol{\eta}(0), \boldsymbol{\eta}(0)) + \|\dot{\mathbf{u}}(0) - \dot{\mathbf{u}}_h(0)\|_0^2 + T^2 \int_0^T \|(I - \Pi_{k-2}^0) \mathbf{f}(\tau)\|_0^2 d\tau \\
&\quad + \frac{h^{2(\mu+1)}}{k^{2m}} \left(\|\dot{\mathbf{u}}\|_{L^2(0, T; [H^{m+1}(\Omega)]^2)}^2 + T^2 \|\ddot{\mathbf{u}}\|_{L^2(0, T; [H^{m+1}(\Omega)]^2)}^2 \right) \\
&\quad + \int_0^\xi \|\dot{\mathbf{v}}_h\|_0^2 dt + \int_0^\xi \|\mathbf{v}_h\|_0^2 dt.
\end{aligned} \quad (106)$$

We estimate the first term in the right-hand side of (106) by using property (26), the definition of $\boldsymbol{\eta}(0)$, adding and subtracting $\mathcal{P}_h \mathbf{u}(0)$, and estimate (83):

$$\begin{aligned}
m_h(\boldsymbol{\eta}(0), \boldsymbol{\eta}(0)) &\leq \mu^* \|\boldsymbol{\eta}(0)\|_0^2 = \mu^* \|\mathbf{u}_h(0) - \mathcal{P}_h \mathbf{u}(0)\|_0^2 \\
&\leq 2\mu^* \|\mathbf{u}_h(0) - \mathbf{u}(0)\|_0^2 + 2\mu^* \|\mathbf{u}(0) - \mathcal{P}_h \mathbf{u}(0)\|_0^2 \\
&\lesssim \|\mathbf{u}_h(0) - \mathbf{u}_0\|_0^2 + \frac{h^{2(\mu+1)}}{k^{2m}} |\mathbf{u}_0|_{m+1}^2.
\end{aligned} \quad (107)$$

We also estimate the last integral term in (106) by using the definition of the $L^2(\Omega)$ -norm, definition (90), Jensen's inequality, and Fubini's Theorem to change the integration order:

$$\begin{aligned}
\|\mathbf{v}_h(t)\|_0^2 &= \int_{\Omega} \left| \int_t^\xi \boldsymbol{\eta}(\tau) d\tau \right|^2 dV \leq \int_{\Omega} |\xi - t| \left(\int_t^\xi |\boldsymbol{\eta}(\tau)|^2 d\tau \right) dV \\
&= |\xi - t| \int_t^\xi \left(\int_{\Omega} |\boldsymbol{\eta}(\tau)|^2 dV \right) d\tau \leq T \int_0^\xi \|\boldsymbol{\eta}(\tau)\|_0^2 d\tau
\end{aligned} \quad (108)$$

and

$$\int_0^\xi \|\mathbf{v}_h(t)\|_0^2 dt = \left(T \int_0^\xi \|\boldsymbol{\eta}(\tau)\|_0^2 d\tau \right) \left(\int_0^\xi dt \right) \leq T^2 \int_0^\xi \|\boldsymbol{\eta}(\tau)\|_0^2 d\tau \quad (109)$$

Using estimates (107) and (108) in (106) and recalling that $\dot{\mathbf{v}}_h = -\boldsymbol{\eta}$, we find that

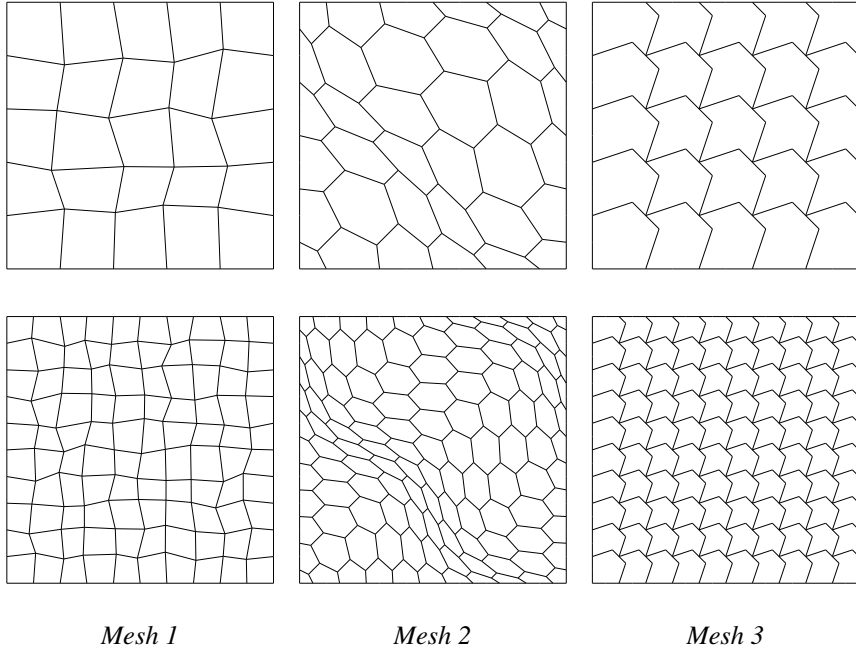


Fig. 2. Base meshes (top row) and first refined meshes (bottom row) of the following mesh families from left to right: randomized quadrilateral mesh; mainly hexagonal mesh; nonconvex octagonal mesh.

$$\begin{aligned}
\|\boldsymbol{\eta}(\xi)\|_0^2 &\lesssim \|\mathbf{u}(0) - \mathbf{u}_h(0)\|_0^2 + \|\dot{\mathbf{u}}(0) - \dot{\mathbf{u}}_h(0)\|_0^2 + T^2 \int_0^T \|(I - \Pi_{k-2}^0) \mathbf{f}(\tau)\|_0^2 d\tau \\
&\quad + \frac{h^{2(\mu+1)}}{k^{2m}} \left(|\mathbf{u}_0|_{m+1}^2 + \|\dot{\mathbf{u}}\|_{L^2(0,T;[H^{m+1}(\Omega)]^2)}^2 + T^2 \|\ddot{\mathbf{u}}\|_{L^2(0,T;[H^{m+1}(\Omega)]^2)}^2 \right) \\
&\quad + (1 + T^2) \int_0^\xi \|\boldsymbol{\eta}(t)\|_0^2 dt.
\end{aligned} \tag{110}$$

An application of Gronwall's inequality yields, for (almost) every $t \in [0, T]$, the desired upper bound on $\boldsymbol{\eta}(t)$:

$$\begin{aligned}
\|\boldsymbol{\eta}(t)\|_0 &\lesssim C(T) \left(\|\mathbf{u}(0) - \mathbf{u}_h(0)\|_0 + \|\dot{\mathbf{u}}(0) - \dot{\mathbf{u}}_h(0)\|_0 + \int_0^T \|(I - \Pi_{k-2}^0) \mathbf{f}(\tau)\|_0 d\tau \right. \\
&\quad \left. + \frac{h^{\mu+1}}{k^m} \left(|\mathbf{u}_0|_{s+1,\Omega} + \|\dot{\mathbf{u}}\|_{L^2(0,T;[H^{m+1}(\Omega)]^2)} + \|\ddot{\mathbf{u}}\|_{L^2(0,T;[H^{m+1}(\Omega)]^2)} \right) \right), \tag{111}
\end{aligned}$$

where $C(T) \simeq \exp(T^3)$ and the constant hidden in the “ \lesssim ” notation depends on μ^* and the mesh regularity constant ϱ , but is independent of h . Finally, we prove the assertion of the theorem through the triangular inequality $\|\mathbf{u}_h - \mathbf{u}\|_0 \leq \|\rho\|_0 + \|\boldsymbol{\eta}\|_0$ and, then, on using (82) to bound ρ and (111) to bound $\boldsymbol{\eta}$. \square

Remark 4.10 *The L^2 estimate in Theorem 4.8 is suboptimal in k because of the suboptimality of the invoked results contained in Lemma 4.2.*

5. Numerical experiments

In this section, we aim to confirm the optimal convergence rate of the numerical approximation of the elastodynamic problem (3)-(7) provided by the virtual element method in accordance with Theorems 4.6 and 4.8. In particular, we let $\Omega = (0, 1)^2$ for $t \in [0, T]$, $T = 1$, and consider initial condition \mathbf{u}_0 , boundary condition \mathbf{g} and forcing term \mathbf{f} determined from the exact solution:

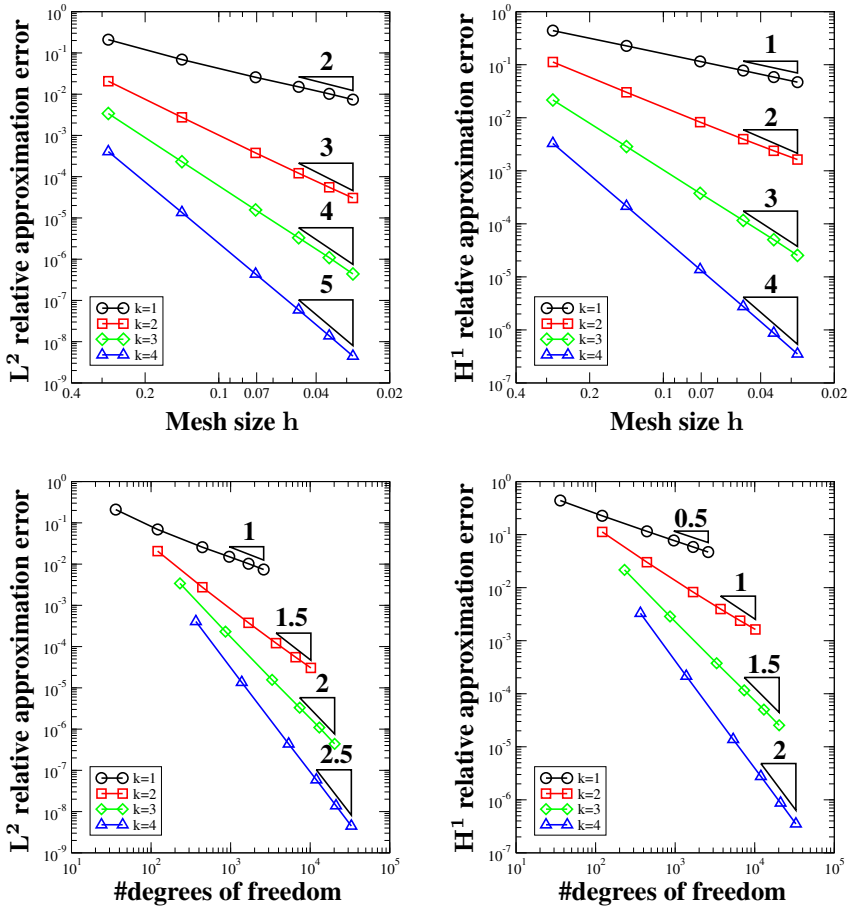


Fig. 3. Convergence plots for the virtual element approximation of Problem (3)-(7) with exact solution (112) using family *Mesh 1* of randomized quadrilateral meshes. Error curves are computed using the L^2 norm (left panels) and H^1 norm (right panels) and are plot versus mesh size h (top panels) and number of degrees of freedom (bottom panels).

$$\mathbf{u}(x, y, t) = \cos\left(\frac{2\pi t}{T}\right) \begin{pmatrix} \sin^2(\pi x) \sin(2\pi y) \\ \sin(2\pi x) \sin^2(\pi y) \end{pmatrix}. \quad (112)$$

To this end, we consider three different mesh partitionings, denoted by:

- *Mesh 1*, randomized quadrilateral mesh;
- *Mesh 2*, mainly hexagonal mesh with continuously distorted cells;
- *Mesh 3*, nonconvex octagonal mesh.

The base mesh and the first refined mesh of each mesh sequence are shown in Figure 2.

These mesh sequences have been widely used in the mimetic finite difference and virtual element literature, and a detailed description of their construction can be found, for example, in [29]. The discretization in time is given by applying the Leapfrog method with $\delta t = 10^{-4}$ and carried out for 10^4 time cycles in order to reach time $T = 1$.

For these calculations, we used the VEM approximation based on the conforming space V_k^h with $k = 2, 3, 4$ and the convergence curves for the three mesh sequences above are reported in Figures 3, 4 and 5. The expected rate of convergence is shown in each panel by the triangle closed to the error curve and indicated by an explicit label. According to Theorem 4.6, we expect that the approximation error decreases as $\mathcal{O}(h^k)$ when using the virtual element method of order k and measuring the error in the H^1 norm. Consistently with our approximation, we also expect to see the approximation error to decrease as $\mathcal{O}(h^{k+1})$ when using the L^2 norm. Furthermore, Figure 6 shows the semilog error curves obtained through a “p”-type refinement calculation for the previous benchmark, i.e for a fixed

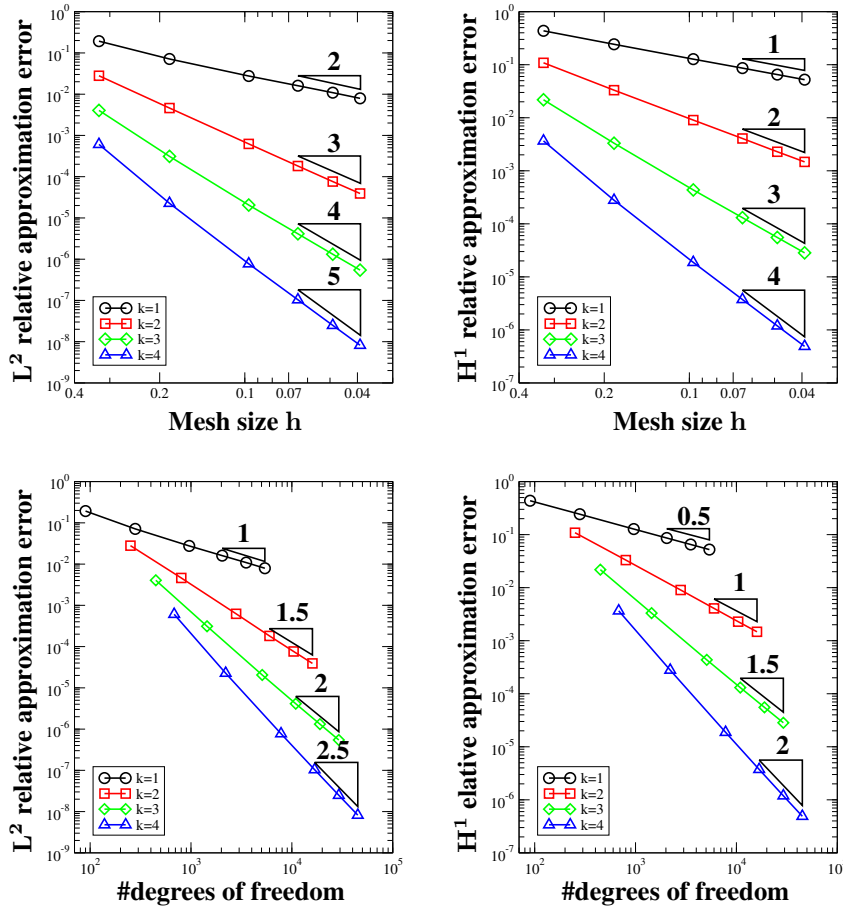


Fig. 4. Convergence plots for the virtual element approximation of Problem (3)-(7) with exact solution (112) using family *Mesh 2* of mainly hexagonal meshes. Error curves are computed using the L^2 norm (left panels) and H^1 norm (right panels) and are plot versus mesh size h (top panels) and number of degrees of freedom (bottom panels).

5×5 mesh of type *I* the order of the virtual element space is increased from $k = 1$ to $k = 10$. We refer the reader to [28] for a detailed presentation of the p/hp virtual element formulations. Here, we compare the performance of the method for two different implementations. In the first one, the space of polynomials of degree k is generated by the standard scaled monomials, while in the second one we consider an orthogonal polynomial basis. Details on the orthogonalization of the basis polynomials are found in [43, 64, 91], where the impact that such a basis can have on the accuracy of the high-order VEM is also discussed. The behavior of the VEM when using nonorthogonal and orthogonal polynomials basis shown in Figure 6 is in accordance with the literature.

These plots confirm that the conforming VEM formulations proposed in this work provide a numerical approximation with optimal convergence rate on a set of representative mesh sequences, including deformed and nonconvex polygonal cells.

6. Conclusions

In this work, we extended the conforming virtual element method for the numerical simulation of two dimensional time-dependent elastodynamics problems. The formulation of the VEM is investigated both theoretically and numerically. From the theoretical side, we proved the stability and the convergence of the semi-discrete approximation in the energy norm and obtain optimal rate of convergence. We also derive L^2 error estimates for the h - and p -refinement. From the numerical side, we assessed the performance of the conforming VEM on a set of different computational

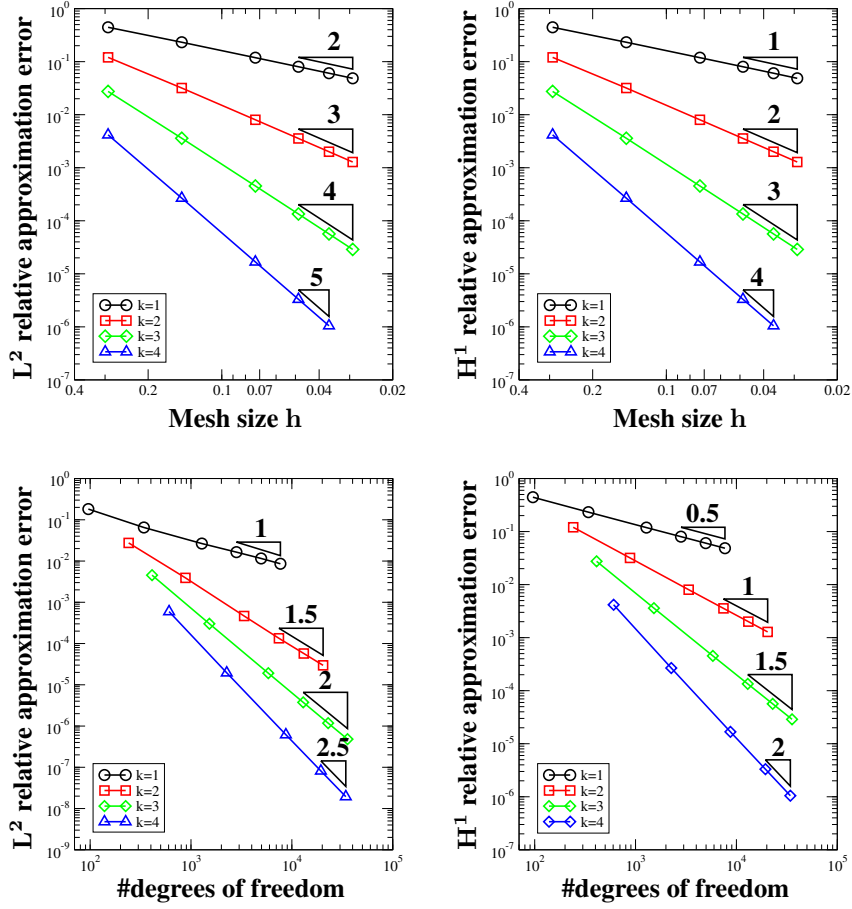


Fig. 5. Convergence plots for the virtual element approximation of Problem (3)-(7) with exact solution (112) using family *Mesh 3* of nonconvex octagonal meshes. Error curves are computed using the L^2 norm (left panels) and H^1 norm (right panels) and are plot versus mesh size h (top panels) and number of degrees of freedom (bottom panels).

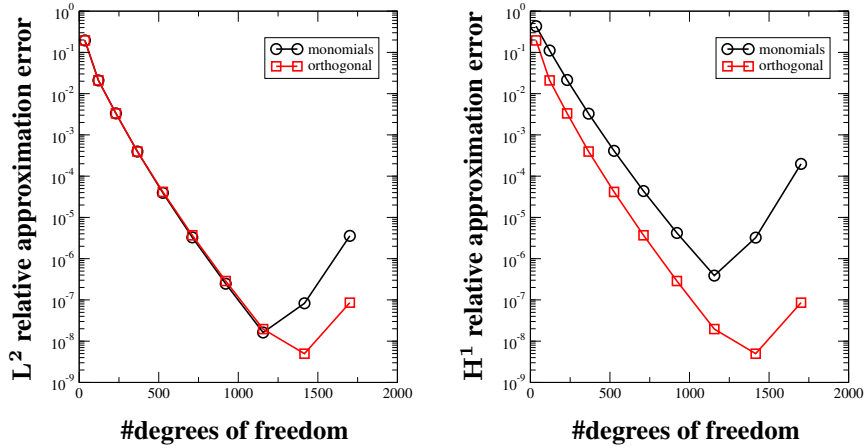


Fig. 6. Convergence plots for the virtual element approximation of Problem (3)-(7) with exact solution (112) using family *Mesh 1* of randomized quadrilateral meshes. Error curves are computed using k-refinement the L^2 norm (left panel) and H^1 norm (right panel) and are plot versus the number of degrees of freedom by performing a refinement of type “p” on a 5×5 mesh. Each plot shows the two convergence curves that are obtained using monomials (circles) and orthogonalized polynomials (squares.)

meshes, including non-convex cells. The theoretical optimal convergence rates in the energy norm are numerically validated, whereas the numerically observed L^2 convergence rates assess the suboptimality of our theoretical L^2 error estimates. Finally, in the p -refinement setting, exponential convergence is experimentally observed.

Acknowledgments

The first and last authors also acknowledge the financial support of PRIN research grant number 201744KLJL “Virtual Element Methods: Analysis and Applications” funded by MIUR and of INdAM-GNCS. The work of the second author was supported by the Laboratory Directed Research and Development (LDRD) Program of Los Alamos National Laboratory under project number 20180428ER. The work of the third author was supported by the LDRD program of Los Alamos National Laboratory under project number 20170033DR. Los Alamos National Laboratory is operated by Triad National Security, LLC, for the National Nuclear Security Administration of U.S. Department of Energy (Contract No. 89233218CNA000001).

References

- [1] D. Adak, E. Natarajan, and S. Kumar. Convergence analysis of virtual element methods for semilinear parabolic problems on polygonal meshes. *Numerical Methods for Partial Differential Equations*, 2018.
- [2] D. Adak, E. Natarajan, and S. Kumar. Virtual element method for semilinear hyperbolic problems on polygonal meshes. *International Journal of Computer Mathematics*, 2018.
- [3] D. Adak and S. Natarajan. Virtual element method for semilinear sine-Gordon equation over polygonal mesh using product approximation technique, 2019. arXiv pre-print N. 1912.05120.
- [4] R. A. Adams and J. J. F. Fournier. *Sobolev spaces*. Pure and Applied Mathematics. Academic Press, 2 edition, 2003.
- [5] B. Ahmad, A. Alsaedi, F. Brezzi, L. D. Marini, and A. Russo. Equivalent projectors for virtual element methods. *Computers & Mathematics with Applications*, 66:376–391, September 2013.
- [6] F. Aldakheel, B. Hudobivnik, A. Hussein, and P. Wriggers. Phase-field modeling of brittle fracture using an efficient virtual element scheme. *Computer Methods in Applied Mechanics and Engineering*, 2018.
- [7] F. Aldakheel, B. Hudobivnik, and P. Wriggers. Virtual element formulation for phase-field modeling of ductile fracture. *International Journal for Multiscale Computational Engineering*, 17, 2019.
- [8] Z. Alterman and F. Karal. Propagation of elastic waves in layered media by finite difference methods. *Bulletin of the Seismological Society of America*, 58(1):367–398, 1968.
- [9] P. Antonietti, A. Ferroni, I. Mazzieri, and A. Quarteroni. hp-version discontinuous galerkin approximations of the elastodynamics equation. *Lecture Notes in Computational Science and Engineering*, 119:3–19, 2017.
- [10] P. F. Antonietti, B. Ayuso de Dios, I. Mazzieri, and A. Quarteroni. Stability analysis of discontinuous Galerkin approximations to the elastodynamics problem. *Journal of Scientific Computing*, 68:143–170, 2016.
- [11] P. F. Antonietti, L. Beirão da Veiga, D. Mora, and M. Verani. A stream virtual element formulation of the stokes problem on polygonal meshes. *SIAM Journal on Numerical Analysis*, 52(1):386–404, 2014.
- [12] P. F. Antonietti, F. Bonaldi, and I. Mazzieri. A high-order discontinuous Galerkin approach to the elasto-acoustic problem. *Comput. Methods Appl. Mech. Engrg.*, 358:112634, 29, 2020.
- [13] P. F. Antonietti, G. Manzini, and M. Verani. The fully nonconforming Virtual Element method for biharmonic problems. *M3AS Math. Models Methods Appl. Sci.*, 28(2), 2018.
- [14] P. F. Antonietti and I. Mazzieri. High-order discontinuous Galerkin methods for the elastodynamics equation on polygonal and polyhedral meshes. *Comput. Methods Appl. Mech. Engrg.*, 342:414–437, 2018.
- [15] P. F. Antonietti, I. Mazzieri, A. Quarteroni, and F. Rapetti. Non-conforming high order approximations of the elastodynamics equation. *Computer Methods in Applied Mechanics and Engineering*, 209:212–238, 2012.
- [16] E. Artioli, S. de Miranda, C. Lovadina, and L. Patruno. A stress/displacement Virtual Element method for plane elasticity problems. *Computer Methods in Applied Mechanics and Engineering*, 325, 2017.
- [17] E. Artioli, S. de Miranda, C. Lovadina, and L. Patruno. A family of virtual element methods for plane elasticity problems based on the Hellinger-Reissner principle. *Computer Methods in Applied Mechanics and Engineering*, 2018.

- [18] B. Ayuso de Dios, K. Lipnikov, and G. Manzini. The non-conforming virtual element method. *ESAIM: Mathematical Modelling and Numerical Analysis*, 50(3):879–904, 2016.
- [19] G. A. Baker, V. A. Dougalis, and O. A. Karakashian. On multistep-Galerkin discretizations of semilinear hyperbolic and parabolic equations. *Nonlinear Analysis: Theory, Methods & Applications*, 4(3):579–597, 1980.
- [20] L. Beirão da Veiga, F. Brezzi, A. Cangiani, G. Manzini, L. D. Marini, and A. Russo. Basic principles of virtual element methods. *Math. Models Methods Appl. Sci.*, 23:119–214, 2013.
- [21] L. Beirão da Veiga, F. Brezzi, and L. D. Marini. Virtual elements for linear elasticity problems. *SIAM Journal on Numerical Analysis*, 51(2):794–812, 2013.
- [22] L. Beirão da Veiga, F. Brezzi, L. D. Marini, and A. Russo. The hitchhiker’s guide to the virtual element method. *Mathematical Models and Methods in Applied Sciences*, 24(8):1541–1573, 2014.
- [23] L. Beirão da Veiga, F. Brezzi, L. D. Marini, and A. Russo. Virtual element methods for general second order elliptic problems on polygonal meshes. *Mathematical Models and Methods in Applied Sciences*, 26(04):729–750, 2015.
- [24] L. Beirão da Veiga, F. Brezzi, L. D. Marini, and A. Russo. H(div) and H(curl)-conforming VEM. *Numerische Mathematik*, 133(2):303–332, 2016.
- [25] L. Beirão da Veiga, F. Brezzi, L. D. Marini, and A. Russo. Mixed virtual element methods for general second order elliptic problems on polygonal meshes. *ESAIM: Mathematical Modelling and Numerical Analysis*, 50(3):727–747, 2016.
- [26] L. Beirão da Veiga, F. Brezzi, L. D. Marini, and A. Russo. Serendipity nodal vem spaces. *Computers and Fluids*, 141:2–12, 2016.
- [27] L. Beirão da Veiga, F. Brezzi, L. D. Marini, and A. Russo. Virtual element methods for general second order elliptic problems on polygonal meshes. *Mathematical Models & Methods in Applied Sciences*, 26(4):729–750, 2016.
- [28] L. Beirão da Veiga, A. Chernov, L. Mascotto, and A. Russo. Basic principles of hp virtual elements on quasiuniform meshes. *Mathematical Models & Methods in Applied Sciences*, 26(8):1567–1598, 2016.
- [29] L. Beirão da Veiga, K. Lipnikov, and G. Manzini. Arbitrary order nodal mimetic discretizations of elliptic problems on polygonal meshes. *SIAM Journal on Numerical Analysis*, 49(5):1737–1760, 2011.
- [30] L. Beirão da Veiga, K. Lipnikov, and G. Manzini. *The Mimetic Finite Difference Method*, volume 11 of *MS&A. Modeling, Simulations and Applications*. Springer, I edition, 2014.
- [31] L. Beirão da Veiga, C. Lovadina, and D. Mora. A Virtual Element Method for elastic and inelastic problems on polytope meshes. *Computer Methods in Applied Mechanics and Engineering*, 295, 10 2015.
- [32] L. Beirão da Veiga, C. Lovadina, and A. Russo. Stability analysis for the virtual element method. *Math. Models Methods Appl. Sci.*, 27(13):2557–2594, 2017.
- [33] L. Beirão da Veiga, C. Lovadina, and G. Vacca. Divergence free virtual elements for the Stokes problem on polygonal meshes. *ESAIM: Mathematical Modelling and Numerical Analysis*, 51(2):509–535, 2017.
- [34] L. Beirão da Veiga and G. Manzini. A virtual element method with arbitrary regularity. *IMA Journal on Numerical Analysis*, 34(2):782–799, 2014. DOI: 10.1093/imanum/drt018, (first published online 2013).
- [35] L. Beirão da Veiga and G. Manzini. Residual a posteriori error estimation for the virtual element method for elliptic problems. *ESAIM: Mathematical Modelling and Numerical Analysis*, 49:577–599, 2015.
- [36] L. Beirão da Veiga, G. Manzini, and M. Putti. Post-processing of solution and flux for the nodal mimetic finite difference method. *Numerical Methods for Partial Differential Equations*, 31(1):336–363, 2015.
- [37] L. Beirão da Veiga, D. Mora, G. Rivera, and R. Rodríguez. A virtual element method for the acoustic vibration problem. *Numerische Mathematik*, 136, 2017.
- [38] M. F. Benedetto, S. Berrone, and A. Borio. The Virtual Element Method for underground flow simulations in fractured media. In *Advances in Discretization Methods*, volume 12 of *SEMA SIMAI Springer Series*, pages 167–186. Springer International Publishing, Switzerland, 2016.
- [39] M. F. Benedetto, S. Berrone, A. Borio, S. Pieraccini, and S. Scialò. A hybrid mortar virtual element method for discrete fracture network simulations. *Journal of Computational Physics*, 306:148–166, 2016.
- [40] M. F. Benedetto, S. Berrone, A. Borio, S. Pieraccini, and S. Scialò. The virtual element method for discrete fracture network flow and transport simulations. In *ECCOMAS Congress 2016 - Proceedings of the 7th European Congress on Computational Methods in Applied Sciences and Engineering*, volume 2, pages 2953–2970, 2016.

- [41] M. F. Benedetto, S. Berrone, S. Pieraccini, and S. Scialò. The virtual element method for discrete fracture network simulations. *Computer Methods in Applied Mechanics and Engineering*, 280(0):135 – 156, 2014.
- [42] M. F. Benedetto, S. Berrone, and S. Scialò. A globally conforming method for solving flow in discrete fracture networks using the Virtual Element Method. *Finite Elements in Analysis and Design*, 109:23–36, 2016.
- [43] S. Berrone and A. Borio. Orthogonal polynomials in badly shaped polygonal elements for the Virtual Element Method. *Finite Elements in Analysis & Design*, 129:14–31, 2017.
- [44] S. Berrone, A. Borio, and S. Scialò. A posteriori error estimate for a PDE-constrained optimization formulation for the flow in DFNs. *SIAM Journal on Numerical Analysis*, 54(1):242–261, 2016.
- [45] S. Berrone, S. Pieraccini, and S. Scialò. Towards effective flow simulations in realistic discrete fracture networks. *Journal of Computational Physics*, 310:181–201, 2016.
- [46] S. Berrone, S. Pieraccini, S. Scialò, and F. Vicini. A parallel solver for large scale DFN flow simulations. *SIAM Journal on Scientific Computing*, 37(3):C285–C306, 2015.
- [47] H. Brezis. *Operateurs maximaux monotones et semi-groupes de contractions dans les espaces de Hilbert*. Number 5 in Mathematical Studies. North-Holland Publishing Company, Amsterdam, 1973.
- [48] F. Brezzi, A. Buffa, and K. Lipnikov. Mimetic finite differences for elliptic problems. *ESAIM: Mathematical Modelling and Numerical Analysis*, 43(2):277–295, 2009.
- [49] F. Brezzi and L. D. Marini. Virtual Element Methods for plate bending problems. *Computer Methods in Applied Mechanics and Engineering*, 253, 2013.
- [50] E. Cáceres, G. N. Gatica, and F. A. Sequeira. A mixed virtual element method for a pseudostress-based formulation of linear elasticity. *Applied Numerical Mathematics*, 2018.
- [51] A. Cangiani, E. H. Georgoulis, T. Pryer, and O. J. Sutton. A posteriori error estimates for the virtual element method. *Numerische Mathematik*, pages 1–37, 2017.
- [52] A. Cangiani, V. Gyrya, and G. Manzini. The non-conforming virtual element method for the Stokes equations. *SIAM Journal on Numerical Analysis*, 54(6):3411–3435, 2016.
- [53] A. Cangiani, V. Gyrya, G. Manzini, and S. O. Chapter 14: Virtual element methods for elliptic problems on polygonal meshes. In K. Hormann and N. Sukumar, editors, *Generalized Barycentric Coordinates in Computer Graphics and Computational Mechanics*, pages 1–20. CRC Press, Taylor & Francis Group, 2017.
- [54] A. Cangiani, G. Manzini, A. Russo, and N. Sukumar. Hourglass stabilization of the virtual element method. *International Journal on Numerical Methods in Engineering*, 102(3-4):404–436, 2015.
- [55] A. Cangiani, G. Manzini, and O. Sutton. The conforming virtual element method for the convection-diffusion-reaction equation with variable coefficients. Technical Report, Los Alamos National Laboratory, 2014. available online at <http://www.osti.gov/scitech/servlets/purl/1159207>.
- [56] A. Cangiani, G. Manzini, and O. Sutton. Conforming and nonconforming virtual element methods for elliptic problems. *IMA Journal on Numerical Analysis*, 37:1317–1354, 2017. (online August 2016).
- [57] O. Certik, F. Gardini, G. Manzini, L. Mascotto, and G. Vacca. The p- and hp-versions of the virtual element method for elliptic eigenvalue problems, 2018. arXiv:1812.09220.
- [58] J. Cheng, A. Shahba, and S. Ghosh. Stabilized tetrahedral elements for crystal plasticity finite element analysis overcoming volumetric locking. *Computational Mechanics*, 57(5):733–753, 2016.
- [59] H. Chi, L. Beirão da Veiga, and G. H. Paulino. Some basic formulations of the virtual element method (VEM) for finite deformations. *Computer Methods in Applied Mechanics and Engineering*, 318, 2017.
- [60] H. Chi, L. Beirão da Veiga, and G. H. Paulino. A simple and effective gradient recovery scheme and a posteriori error estimator for the Virtual Element Method (VEM). *Computer Methods in Applied Mechanics and Engineering*, 2018.
- [61] H. Chi, L. Beirão da Veiga, and G. H. Paulino. Some basic formulations of the virtual element method (VEM) for finite deformations. *Computer Methods in Applied Mechanics and Engineering*, 318:148–192, 2017.
- [62] H. Chi, A. Pereira, I. F. M. Menezes, and G. H. Paulino. Virtual element method (vem)-based topology optimization: an integrated framework. *Structural and Multidisciplinary Optimization*, 2019.
- [63] R. Courant, K. Friedrichs, and H. Lewy. Über die partiellen differenzengleichungen der mathematischen physik. *Mathematische annalen*, 100(1):32–74, 1928.
- [64] F. Dassi and L. Mascotto. Exploring high-order three dimensional virtual elements: bases and stabilizations. *Comput. Math. Appl.*, 75(9):3379–3401, 2018.
- [65] J. D. De Basabe, M. K. Sen, and M. F. Wheeler. The interior penalty discontinuous Galerkin method for elastic

wave propagation: grid dispersion. *Geophysical Journal International*, 175(1):83–93, 2008.

[66] M. L. De Bellis, P. Wriggers, and B. Hudobivnik. Serendipity virtual element formulation for nonlinear elasticity. *Computers & Structures*, 223, 2019.

[67] M. L. De Bellis, P. Wriggers, B. Hudobivnik, and G. Zavarise. Virtual element formulation for isotropic damage. *Finite Elements in Analysis and Design*, 144, 2018.

[68] E. A. De Souza Neto, F. M. A. Pires, and D. R. J. Owen. F-bar-based linear triangles and tetrahedra for finite strain analysis of nearly incompressible solids. Part I: formulation and benchmarking. *International Journal for Numerical Methods in Engineering*, 62(3):353–383, 2005.

[69] V. Dhanush and S. Natarajan. Implementation of the virtual element method for coupled thermo-elasticity in abaqus. *Numerical Algorithms*, 2018.

[70] D. A. Di Pietro, J. Droniou, and G. Manzini. Discontinuous skeletal gradient discretisation methods on polytopal meshes. *Journal of Computational Physics*, 355:397–425, 2018.

[71] M. Dumbser and M. Käser. An arbitrary high-order discontinuous Galerkin method for elastic waves on unstructured meshes – II. The three-dimensional isotropic case. *Geophysical Journal International*, 167(1):319–336, 2006.

[72] E. Faccioli, F. Maggio, R. Paolucci, and A. Quarteroni. 2D and 3D elastic wave propagation by a pseudo-spectral domain decomposition method. *Journal of Seismology*, 1(3):237–251, 1997.

[73] E. Faccioli, F. Maggio, A. Quarteroni, and A. Tagliani. Spectral-domain decomposition methods for the solution of acoustic and elastic wave equations. *Geophysics*, 61(4):1160–1174, 1996.

[74] A. Ferroni, P. F. Antonietti, I. Mazzieri, and A. Quarteroni. Dispersion-dissipation analysis of 3D continuous and discontinuous spectral element methods for the elastodynamics equation. *MOX Report 18/2016, submitted*, 2016.

[75] A. Frankel. Three-dimensional simulations of ground motions in the San Bernardino valley, California, for hypothetical earthquakes on the San Andreas fault. *Bulletin of the Seismological Society of America*, 83(4):1020–1041, 1993.

[76] A. L. Gain, C. Talischi, and G. H. Paulino. On the Virtual Element Method for three-dimensional linear elasticity problems on arbitrary polyhedral meshes. *Computer Methods in Applied Mechanics and Engineering*, 282, 2014.

[77] J. S. Hesthaven. From electrostatics to almost optimal nodal sets for polynomial interpolation in a simplex. *SIAM Journal on Numerical Analysis*, 35(2):655–676, 1998.

[78] B. Hudobivnik, F. , and P. . A low order 3D virtual element formulation for finite elastoplastic deformations. *Computational Mechanics*, 2018.

[79] A. Hussein, F. Aldakheel, B. Hudobivnik, P. Wriggers, P.-A. Guidault, and O. Allix. A computational framework for brittle crack-propagation based on efficient virtual element method. *Finite Elements in Analysis and Design*, 159, 2019.

[80] A. Hussein, B. Hudobivnik, F. Aldakheel, P. Wriggers, P.-A. Guidault, and O. Allix. A virtual element method for crack propagation. *PAMM*, 18, 2018.

[81] H. Igel. Wave propagation in three-dimensional spherical sections by the Chebyshev spectral method. *Geophysical Journal International*, 136(3):559–566, 1999.

[82] M. Käser and M. Dumbser. An arbitrary high-order discontinuous Galerkin method for elastic waves on unstructured meshes – I: The two-dimensional isotropic case with external source terms. *Geophysical Journal International*, 166(2):855–877, 2006.

[83] D. Komatitsch and J. Tromp. Introduction to the spectral element method for three-dimensional seismic wave propagation. *Geophysical Journal International*, 139(3):806–822, 1999.

[84] D. Kosloff, D. Kessler, A. Filho, E. Tessmer, A. Behle, and R. Strahilevitz. Solution of the equations of dynamic elasticity by a Chebychev spectral method. *Geophysics*, 55(6):734–748, 1990.

[85] D. D. Kosloff and E. Baysal. Forward modeling by a Fourier method. *Geophysics*, 47(10):1402–1412, 1982.

[86] K. Lipnikov and G. Manzini. A high-order mimetic method for unstructured polyhedral meshes. *Journal of Computational Physics*, 272:360–385, 2014.

[87] K. Lipnikov, G. Manzini, and M. Shashkov. Mimetic finite difference method. *Journal of Computational Physics*, 257 – Part B:1163–1227, 2014. Review paper.

[88] G. Manzini, K. Lipnikov, J. D. Moulton, and M. Shashkov. Convergence analysis of the mimetic finite dif-

ference method for elliptic problems with staggered discretizations of diffusion coefficients. *SIAM Journal on Numerical Analysis*, 55(6):2956–2981, 2017.

[89] G. Manzini, A. Russo, and N. Sukumar. New perspectives on polygonal and polyhedral finite element methods. *Mathematical Models & Methods in Applied Sciences*, 24(8):1621–1663, 2014.

[90] M. Marino, B. Hudobivnik, and P. Wriggers. Computational homogenization of polycrystalline materials with the Virtual Element Method. *Computer Methods in Applied Mechanics and Engineering*, 355, 2019.

[91] L. Mascotto. Ill-conditioning in the virtual element method: stabilizations and bases. *Numer. Methods Partial Differential Equations*, 34(4):1258–1281, 2018.

[92] P. Moczo, J. Kristek, and M. Gális. *The Finite-Difference Modelling of Earthquake Motions: Waves and Ruptures*. Cambridge University Press, 2014.

[93] D. Mora and G. Rivera. A priori and a posteriori error estimates for a virtual element spectral analysis for the elasticity equations. *IMA Journal of Numerical Analysis*, 2018.

[94] D. Mora, G. Rivera, and R. Rodríguez. A virtual element method for the Steklov eigenvalue problem. *Mathematical Models and Methods in Applied Sciences*, 25(08):1421–1445, 2015.

[95] S. Natarajan, P. A. Bordas, and E. T. Ooi. Virtual and smoothed finite elements: a connection and its application to polygonal/polyhedral finite element methods. *International Journal on Numerical Methods in Engineering*, 104(13):1173–1199, 2015.

[96] V. M. Nguyen-Thanh, X. , H. , T. Rabczuk, and P. Wriggers. A virtual element method for 2D linear elastic fracture analysis. *Computer Methods in Applied Mechanics and Engineering*, 2018.

[97] K. B. Olsen and R. J. Archuleta. Three-dimensional simulation of earthquakes on the Los Angeles fault system. *Bulletin of the Seismological Society of America*, 86(3):575–596, 1996.

[98] K. Park, H. Chi, and G. H. Paulino. On nonconvex meshes for elastodynamics using virtual element methods with explicit time integration. *Computer Methods in Applied Mechanics and Engineering*, 356, 2019.

[99] K. Park, H. Chi, and G. H. Paulino. Numerical recipes for elastodynamic virtual element methods with explicit time integration. *Int. J. Numer. Methods Eng.*, 121, 2020.

[100] G. H. Paulino and A. L. Gain. Bridging art and engineering using Escher-based virtual elements. *Structures and Multidisciplinary Optimization*, 51(4):867–883, 2015.

[101] I. Perugia, P. Pietra, and A. Russo. A plane wave virtual element method for the Helmholtz problem. *ESAIM: Mathematical Modelling and Numerical Analysis*, 50(3):783–808, 2016.

[102] A. Quarteroni, R. Sacco, and F. Saleri. *Numerical Mathematics*, volume 37 of *Texts in Applied Mathematics*. Springer, 2007.

[103] A. Quarteroni, A. Tagliani, and E. Zampieri. Generalized Galerkin approximations of elastic waves with absorbing boundary conditions. *Computer Methods in Applied Mechanics and Engineering*, 163(1–4):323 – 341, 1998.

[104] P.-A. Raviart and J.-M. Thomas. *Introduction à l’analyse numérique des équations aux dérivées partielles*. Collection Mathématiques Appliquées pour la Maîtrise. [Collection of Applied Mathematics for the Master’s Degree]. Masson, Paris, 1983.

[105] B. D. Reddy and D. van Huyssteen. A virtual element method for transversely isotropic elasticity. *Computational Mechanics*, 2019.

[106] B. Rivière and M. F. Wheeler. Discontinuous finite element methods for acoustic and elastic wave problems. *Contemporary Mathematics*, 329:271–282, 2003.

[107] G. Seriani, E. Priolo, and A. Pregarz. Modelling waves in anisotropic media by a spectral element method. In *Proceedings of the third international conference on mathematical and numerical aspects of wave propagation*, pages 289–298. SIAM, 1995.

[108] J. Sorić, P. Wriggers, and O. Allix. Finite and virtual element formulations for large strain anisotropic material with inextensive fibers. In *Multiscale Modeling of Heterogeneous Structures*, volume 86 of *Lecture Notes in Applied and Computational Mechanics*, chapter Chapter 11. Springer International Publishing, 2018.

[109] M. A. Taylor, B. Wingate, and R. Vincent. An algorithm for computing Fekete points in the triangle. *SIAM Journal on Numerical Analysis*, 38(5):1707–1720, 2000.

[110] G. Vacca. Virtual element methods for hyperbolic problems on polygonal meshes. *Computers & Mathematics with Applications*, 2016.

[111] G. Vacca and L. Beirão da Veiga. Virtual element methods for parabolic problems on polygonal meshes.

Numerical Methods for Partial Differential Equations. An International Journal., 31(6):2110–2134, 2015.

[112] P. A. J. Van Den Bogert, R. De Borst, G. T. Luijen, and J. Zeilmaker. Roust finite elements for 3Danalysys of rubber-like materials. *Engineering Computations*, 8(1):3–17, 1991.

[113] T. Warburton. An explicit construction of interpolation nodes on the simplex. *Journal of Engineering Mathematics*, 56(3):247–262, 2006.

[114] P. Wriggers and B. Hudobivnik. A low order virtual element formulation for finite elasto-plastic deformations. *Computer Methods in Applied Mechanics and Engineering*, 10 2017.

[115] P. Wriggers, B. D. Reddy, W. Rust, and B. Hudobivnik. Efficient virtual element formulations for compressible and incompressible finite deformations. *Computational Mechanics*, 2017.

[116] P. Wriggers and W. T. Rust. A virtual element method for frictional contact including large deformations. *Engineering Computations*, 2019.

[117] P. Wriggers, W. T. Rust, and B. D. Reddy. A virtual element method for contact. *Computational Mechanics*, 58, 2016.

[118] E. Zampieri and A. Tagliani. Numerical approximation of elastic waves equations by implicit spectral methods. *Computer Methods in Applied Mechanics and Engineering*, 144(1):33–50, 1997.

[119] B. Zhang and M. Feng. Virtual element method for two-dimensional linear elasticity problem in mixed weakly symmetric formulation. *Applied Mathematics and Computation*, 328, 2018.

[120] B. Zhang, J. Zhao, Y. Yang, and S. Chen. The nonconforming virtual element method for elasticity problems. *Journal of Computational Physics*, 2018.

[121] J. Zhao, S. Chen, and B. Zhang. The nonconforming virtual element method for plate bending problems. *Mathematical Models & Methods in Applied Sciences*, 26(9):1671–1687, 2016.